Department of Precision and Microsystems Engineering

Structured Illumination Imaging and Improvements in Scattering Medium

Jingwen Hu

Report no	:	2023.056
Coach	:	I.C. (Inge) van der Knijff
Professor	:	Dr.ir. S. (Sophinese) Iskander-Rizk
Specialisation	:	Optics
Type of report	:	MSc Thesis
Date	:	17 August 2023

TU Delft
Delft University of Technology

Structured Illumination Imaging and Improvements in Scattering Medium

STRUCTURED ILLUMINATION IMAGING AND IMPROVEMENTS IN SCATTERING MEDIUM

to obtain the degree of Master
at Delft University of Technology,
to be defended in on Thursday 24 August 2023

Jingwen HU

Supervisors:
Sophinese Iskander-Rizk, (TU Delft, 3ME faculty)
Inge van der Knijff, (TU Delft, 3ME faculty)

Chair:
Nandini Bhattacharya, (TU Delft, 3ME faculty)

Contents

Abstract

Bio-imaging plays an essential role in life sciences and medicine. Recently, structured illumination has emerged as a promising super-resolution technique. However, in the case of thick scattering media, the benefits of structured illumination can be significantly reduced compared to conventional illumination methods, resulting in significant degradation of imaging quality. Therefore, the question of dealing with the challenges posed by structured illumination in scattering media has become a topic of considerable focus. In this thesis, an experimental setup aimed at achieving super-resolution imaging using structured illumination is developed. The factors influencing the imaging process are systematically analyzed. At the same time, machine learning methods for recovering structured illumination patterns propagated through scattering media are explored. Overall, this research tackles the challenge of improving super-resolution imaging through scattering medium thereby contributing to the development of biological and medical imaging technologies.

1

INTRODUCTION

This chapter describes the principles of structured illumination. Thereby, the scattering problem of structured illumination that needs to be improved is derived. Finally, motivation and research questions behind this work are derived based on the analysis in this chapter.

1.1. STRUCTURED ILLUMINATION

This section describes the principles of structured illumination and the different kinds of applications. The advantages and disadvantages of super-resolution optical structured illumination are discussed.

1.1.1. STRUCTURED ILLUMINATION MICROSCOPY

Structured illumination microscopy (SIM) has been developed as a wide-field illumination technique for achieving higher resolution[1]. There are many applications of SIM. Optical sectioning, super-resolution, surface profiling, and phase imaging are the four common types of SIM[1].

Different SIM technologies have different capabilities and different applications. Optical sectioning is a three-dimensional imaging technique. It can be used for applications in 3D imaging of cell cores and chromosomes[1]. Super-resolution is a method of increasing resolution, and it has extensive applications in vivo cell imaging[2]. Surface profiling and phase imaging use the principle of interference of light for non-contact imaging[1].

1.1.2. SUPER-RESOLUTION STRUCTURED ILLUMINATION

Super-resolution structured illumination microscopy(SR-SIM) allows for probing higher spatial frequencies and therefore achieves higher resolution than conventional microscopy. SR-SIM is a method of increasing resolution by illuminating the sample with spatially structured excitation light. High-resolution information that is frequently unavailable is depicted in the observed picture, which resembles Moire fringes[3].

Regarding the principle of SR-SIM, it can be understood first in terms of moiré. The increase in resolution originates from the higher spatial frequencies excited thanks to the chosen illumination patterns. Figure1.1 shows that when a sample is illuminated by an illumination pattern with high spatial frequencies, the high frequencies in the illumination pattern and the sample are mixed together. This mixing produces a pattern that could be detected at a lower frequency.

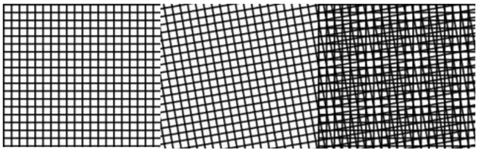

Figure 1.1: Frequency transfer principle

There are many types of SR-SIM, including wide-field SIM, spot-scanning SIM using different illumination patterns[4]. Due to its high resolution and ability to integrate well with other technologies, SR-SIM has many applications, including live cell dynamics and lymphoid tissue[5]. To obtain the resolution improvement, several images with different structured illumination patterns are collected[1]. The collection of images is used in a reconstruction algorithm to produce high-resolution images. Sinusoidal fringes are a commonly used structured illumination pattern. Figure1.2 shows an example of super-resolution imaging. The object is illuminated by three different phase shifted and then reconstructed to obtain the final image.

However, it is challenging to perform SR-SIM in scattering media. In thick scattering specimens, the resolution of SIM imaging is greatly affected by the scattering[6][7][8][9]. The main reason is that more significant scattering degrades the illumination structure and increases background[10]. This disadvantage of SR-SIM will cause many problems. For example, SIM artifacts are caused by scattering in thick samples[6]. Aberrations cause this artifact due to scattering of the excitation light on the sample[6]. In addition, the scattering problem will reduce imaging depth[8][11]. In conclusion, the scattering problem affects SIM.

An example of the effect of scattering on structural lighting is given below. Photoacoustic microscopy(PAM) is a biomedical imaging technique with many applications in biomedicine. As shown in figure1.3, the left side is a combined photoacoustic imaging

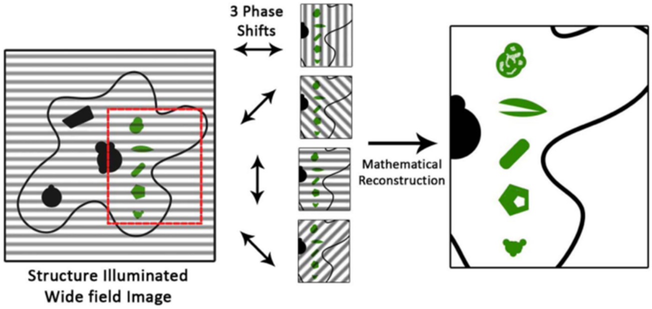

Figure 1.2: Super-resolution imaging[1]

and structural illumination technique (SIR-PAM), and the right side is a conventional photoacoustic imaging technique. We can find that imaging in the scattering medium depth of 4 centimetres and above is significantly affected, resulting from the structural illumination being affected by the scattering medium[12].

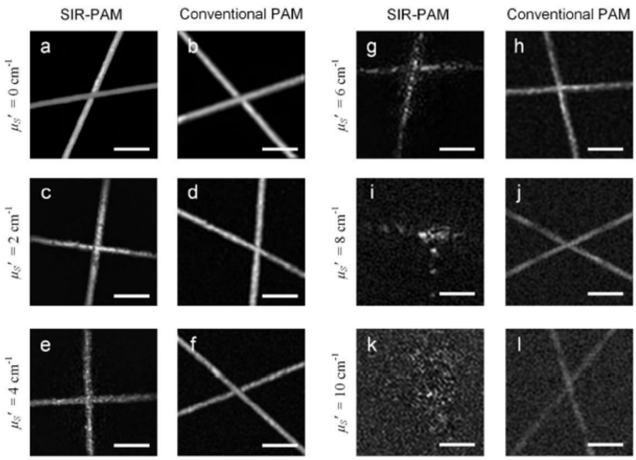

Figure 1.3: Scattering Effects on Structural Lighting Techniques[12]

1.2. RESEARCH MOTIVATION AND OBJECTIVES

In the first section, we concluded that scattering would affect SIM [10] by causing artefacts[6] and reducing imaging depth[8][11].

Furthermore, combinations of structured illumination and photoacoustic microscopy(PAM) also have problems in scattering while improving imaging capabilities and solving the out-of-focus problem[12][13][14][15]. This combined technology is more easily affected by scattering than conventional PAM[12]. Consequently, although structured illumination can improve photoacoustic imaging, the combined technology has similar disadvantages in scattering. So improving the SR-SIM in the scattering medium is a direction worth studying. The crucial aspect of this problem is to address the effect of the scattering medium on the structure illumination.

As a result, the first question of this research is to study how to realize structured illumination and how it will propagate in the scattering medium. Therefore, the first step of the research question is to realize a structured illumination microscope. The second question is how to improve the structured illumination in the scattering medium based on the first step. In order to study the research questions, two hypotheses were set up. This study hypothesizes that the propagation of structural illumination in media is regular and learnable, and the second hypothesis is that we can improve the imaging performance of structured illumination in scattering media by correcting the propagation of structural illumination in media by physical or computer means.

1.3. OUTLINE OF THESIS

The first chapter of this thesis is an introduction, which mainly introduces the structured illumination technology on which this paper is based and also writes the research motivation. The second chapter is the realization of structured illumination light, which introduces the optical principle of structured illumination and the method of realizing it through spatial light modulators. Moreover, the zero-order diffraction problem encountered in the realization process and its solution are shown, and the experimental setup for realizing structured illumination is obtained. The third chapter is the realisation of structured illumination imaging. It introduces the principle of structured illumination imaging and the principle of the algorithm for reconstructing the image. In terms of experiments, chapter three researches the effects of different experimental setups, illumination pattern angles and frequencies on the imaging. Chapter four is to study how to improve the structural illumination pattern in scattering medium, mainly through the machine learning method to study the inverse scattering equation, thus obtaining the before-scattering illumination pattern through the after-scattering illumination pattern. Chapter five is a discussion and outlook, which analyses what is worth improving in the results of this thesis, while pointing out the directions worth researching in the future.

2

STRUCTURED ILLUMINATION LIGHT REALIZATION

This chapter obtains structured illumination patterns by using spatial light modulators and compares other methods that can be used to obtain structured illumination patterns. Moreover, this chapter starts from the basic Maxwell's equations and explains the diffraction and zero-order diffraction theories involved in this thesis. Furthermore, the experimental instruments and setups designed are introduced. Lastly, the results of the experiments are shown.

2.1. METHODS TO OBTAIN ILLUMINATED LIGHT PATTERNS

The section describes the realization of structured illumination that can be projected on the observed object. The first step is to generate structured illumination light. There are several ways to generate structured illumination light, including spatial light modulators and gratings. In this study, we used Spatial Light Modulators, of which the operating principles will be discussed in the next section.

2.1.1. SPATIAL LIGHT MODULATORS (SLMS)

Spatial light modulators (SLMs) offer fine-grained light control, with ability to create 2D light patterns with modifiable features[16]. The SLM is a real-time reconfigurable device capable of modifying the phase or polarisation of the optical wavefront.[17]. SLMs are employed in a variety of fields, such as display technology, optical imaging, holography, laser beam shaping, adaptive optics, and optical manipulation[18].

Depending on the existing research, multiple techniques are used by SLM to control light. SLM based on liquid crystals works using their voltage-dependent refractive index[19]. These SLMs comprise an array of pixels, each containing a liquid crystal element. The refractive index of each pixel can be changed by applying an electric field to the liquid crystal components. The incident light's phase, polarization, or intensity can change due to this modification of the refractive index[19]. Digital micromirror device (DMD) are another type of light modulator, on the other hand, are based on an array of microscopically small mirrors. By selectively tilting the mirrors, the incident light can be spatially modulated, allowing for precise control over the intensity distribution or phase modulation[20].

For over a decade, liquid crystal spatial light modulators (LC-SLMs) have emerged as the preferred options in shaping wavefront, establishing themselves as the dominant solution in complex photonics applications. LC-SLMs typically offer the ability to modify the wavefront phase with the ranging from 8 to 12 bits[21]. Consequently, LC-SLMs are more frequently employed to achieve structured illumination and generate exact structural patterns. Therefore, LC-SLMs are suited for the experimental requirements presented in this study.

2.1.2. OTHER METHODS FOR OBTAINING STRUCTURED ILLUMINATION PATTERNS

In addition to SLMs, there are alternative techniques available for generating structured illumination patterns. We can classify these techniques into grating-based and laser-based methods.

Grating-based techniques are commonly employed for the generation of structured illumination patterns. Binary Ronchi gratings consist of alternating transparent and opaque stripes of equal width. When exposed to collimated light, they produce distinct bright and dark stripes on the surface of the object[22]. On the other hand, laser-based techniques offer an alternative avenue for achieving structured illumination. Scanning laser projectors utilize a moving laser beam to scan the surface of the object, resulting in the creation of structured illumination patterns. The specimen is illuminated by a series of streaks rather than uniform lighting. This is achieved by rapidly scanning different planes within the sample using a narrow laser beam, while simultaneously capturing the image using a camera[23].

To summarize, each approach offers advantages and limitations. In the context of previous literature, grating methods are relatively straightforward to implement and are suitable for static pattern generation. However, they may have limitations in terms of flexibility in pattern design and modification. On the other hand, laser scanning techniques involve a more complex experimental setup. Considering the need for high-resolution illumination patterns, particularly in super-resolution imaging applications, LC-SLMs emerge as the optimal choice. LC-SLMs allow for precise control over various pattern parameters, such as phase, intensity, and polarization, while also offering flexibility in pattern design. However, the use of LC-SLMs may require calibration procedures to ensure accurate performance.

2.2. OPTICAL THEORY ANALYSIS

This section introduces the theory of Fourier optics and the theory of zero-order diffraction. Fourier optics starts with Maxwell's equations and proceeds to Fraunhofer diffraction, which is used in this thesis. Additionally, the theory of Fourier optics for the lenses is also presented. Finally, the theory of zero-order diffraction and the solution of zero-order diffraction are presented.

2.2.1. FOURIER OPTICS

We have selected SLM to produce structured illumination light. The primary imaging method of SLM is to use the diffraction principle through phase modulation. One of the uses of SLM is modulating the incident light into a diffraction pattern of the desired pattern, thus obtaining the desired pattern after a Fourier transform. The main benefit of diffraction patterns is using all available degrees of freedom to manipulate the beam. Therefore, we need first to explain the diffraction principle and then theoretically analyze the diffraction mode of SLM according to the optical principle. Moreover, lenses are also used in the construction of the experiment setup. Thus, the effect of the lens on the diffracted light also needs to be analyzed theoretically.

The structure of this section is as follows. The first two paragraphs of this section are devoted to the theoretical analysis of the diffraction of the SLM; the third paragraph is devoted to the elucidation of the Fourier optics of the lenses, and the fourth paragraph is devoted to the analysis at the level of the Fourier optics of the optical system consisting of the lenses that are going to be used in the experiments (4F system).

SCALAR THEORY OF DIFFRACTION

Diffraction phenomena play a pivotal role in the examination of wave propagation. Diffraction can be understood as any phenomenon in which light deviates from its straight path of propagation which cannot be explained by reflection or refraction. It arises when the transverse width of a light wave is confined, and its impact becomes prominent when the confinement scale approaches the wavelength of the radiation used. Consequently, the application of diffraction theory holds significant importance in the optical experiments conducted in this study. Remarkably, the pronounced manifestation of diffraction phenomena is anticipated in the present experiment involving micron-level modulation using a SLM. Furthermore, the utilization of SLM exemplifies the practical application of diffraction theory. By harnessing the principles of diffraction, SLM enables the formation of images through the redistribution of light. This characteristic of SLM leads to excellent light efficiency advantages, enhancing the performance and functionality of optical systems.

Scalar wave equation Light is an electromagnetic wave, so Maxwell's equations are the most fundamental starting point for analysis. In the case where the propagating medium is linear, isotropic, homogeneous, and free of dispersion, Maxwell's equations can be expressed as a scalar wave equation as follow, where $u(P,t)$ is any scalar field component, n is the refractive index, and c is the speed of light in vacuum. Moreover, P stands for spatial location, and t for time.

$$\Delta^2 u(P,t) - \frac{n^2}{c^2}\frac{\partial^2 u(P,t)}{\partial t^2} = 0 \tag{2.1}$$

The light in the experiments in this study propagates mainly in air and the lens, which satisfies the conditions of the wave equation. For the analysis and synthesis of SLMs, scalar diffraction theory is appropriate since the liquid crystals in SLMs can be considered homogeneous and only use a small diffracted angle.

Introducing $u(P,t)$as the case of light perturbation at moment t at point P, and introducing $U(P)$ as a complex-valued function of position and v as the frequency of the light. Bringing the relationship $u(P,t) = ReU(P)exp(-j2\pi vt)$ between u and U into the above equation, the following Helmholtz equation can be obtained. We will obtain the diffraction pattern after solving this equation 2.2[24].

$$(\Delta^2 + k^2)U(P) = 0 \tag{2.2}$$

Where k is the wave number:

$$k = 2\pi n\frac{v}{c} = \frac{2\pi}{\lambda} \tag{2.3}$$

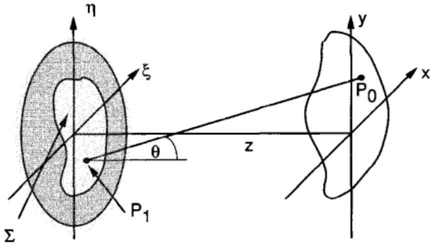

Figure 2.1: Geometric relations of diffraction[24]

Fraunhofer diffraction The right-angle coordinate system is shown in the figure2.1, and the diffracted aperture is in the plane (ξ,η),Illuminated by light in the forward z-direction. Define the length of the vector of P_0 pointing to the point P_1 as r_{01}. We will calculate the wave field in the plane (x,y) parallel to the plane (ξ,η) and at a distance z normal to it. If the following stronger approximation conditions are satisfied[24]:

$$z \gg \frac{k(\xi^2+\eta^2)_{max}}{2} \tag{2.4}$$

the propagation of light can be described by the Fraunhofer diffraction integral in equation2.5, and the observed field strength can be derived directly from the Fourier transform of the field distribution over the aperture itself.[24]. When The observation point (screen or detector) is far from the diffracting aperture or object, the Fraunhofer diffraction integral turns into a Fourier Transform, which is also called Far-field approximation.

$$U(x,y,z) = \frac{e^{jkz} e^{j\frac{k}{2z}(x^2+y^2)}}{j\lambda z} \int\int_{-\infty}^{\infty} U(\xi,\eta,0) exp[-j\frac{2\pi}{\lambda z}(x\xi + y\eta)] d\xi d\eta \tag{2.5}$$

In conclusion, the Fraunhofer diffraction was used in this study. This is because the experiments in this study meet the Fraunhofer approximation. In the experiment, the diffraction aperture is estimated by the diffraction pattern of SLM. We estimate the diffraction aperture to be one pixel(a = $8\mu m$) of the SLM, and the laser wavelength used in the experiment is $\lambda = 1550nm$. Fresnel approximation occurs when the diffraction imaging distance is less than $41.3 \times 10^{-6}m$. The "antenna designer's formula" $z \geq \frac{2a^2}{\lambda}$ shows that the Fraunhofer approximation is satisfied when the imaging distance is more significant than $82.6 \times 10^{-6}m$. This paper's experimental setup is within 1m, so the Fraunhofer approximation is assumed to be suitable.

FOURIER TRANSFORMING PROPERTIES OF LENSES

Lenses are essential elements in optical systems and are analyzed below through wave optics. The results of this approach are identical to those of geometrical optics and allow for diffraction effects which have an important influence on this experiment.

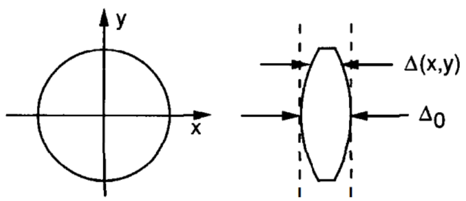

Figure 2.2: Front view (left) and side view (right) of the lens, and thickness function

Phase change of the lens First, we define the lens and the incident light. Suppose a ray of light is incident on a thin lens from the point(x,y). Ignore the lateral translation of the light at this point. The lens is shown in the figure2.2, and the lens thickness at the coordinates (x,y) is $\Delta(x,y)$, maximum thickness is Δ_0. We were approximating the sphere of the lens with a paraboloid so that the thickness function $\Delta(x,y) = \Delta_0 - \frac{x^2+y^2}{2}(\frac{1}{R_1} - \frac{1}{R_2})$. For the focal length, we know that $\frac{1}{f} = (n-1)(\frac{1}{R_1} - \frac{1}{R_2})$. The resulting phase delay due to free space $kn\Delta(x,y)$ and the lens $k[\Delta_0 - \Delta(x,y)]$ can be equivalently expressed as a phase change equation2.6.

$$t_l(x,y) = exp[-j\frac{k}{2f}(x^2+y^2)] \tag{2.6}$$

Fourier transformation of the lens The phase change produced by the lens also performs a Fourier transform operation under certain conditions, which is analyzed in the following section.

The experimental setup in this study can be summarised in a model: the input(SLM) is located at a distance d in front of the lens, as shown in the figure2.3.

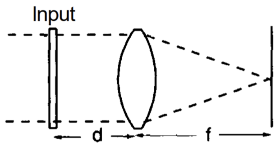

Figure 2.3: Geometry for performing the Fourier transform operation with a positive lens

In analyzing this optical model, we start with a few assumptions. Let the input transparency have an amplitude transmittance of $t_A(x,y)$ and be placed before a converging lens with focal length f, which is shown in figure2.3. Assuming that the input is uniformly illuminated by a vertical unicolour plane wave with an amplitude A, which is the most desirable way of experimentally illuminating the SLM with the laser. At this point, the light perturbation incident on the lens is:

$$U_l(x,y) = At_A(x,y) \tag{2.7}$$

In addition, let $F_o(f_X, f_Y)$ represent the Fourier spectrum of the light transmitted by the input transparency. Let the light pupil function $P(x,y)$ denote the limited size of the lens aperture, and when inside the lens aperture, $P(x,y) = 1$.Using the equation2.6, the amplitude distribution immediately behind the lens is:

$$U_l^{'}(x,y) = U_l(x,y)P(x,y)exp[-j\frac{k}{2f}(x^2+y^2)] \tag{2.8}$$

The imaging in this study is all in the focal plane. Field amplitude distribution in the focal plane $U_f(u,v)$ behind the lens can be found by using the Fresnel diffraction formula. Let $d = f$, The quadratic phase factor in equation2.8 can be canceled out with that in the Fresnel formula.

$$\begin{aligned} &U_f(u,v) = \frac{exp[j\frac{k}{2f}(1-\frac{d}{f})(u^2+v^2)]}{j\lambda f}F_o(\frac{u}{\lambda f},\frac{v}{\lambda f}) \\ &or \\ &U_f(u,v) = \frac{exp[j\frac{k}{2f}(1-\frac{d}{f})(u^2+v^2)]}{j\lambda f} \times \int\int_{-\infty}^{\infty} t_A(\xi,\eta)exp[-j\frac{2\pi}{\lambda f}(\xi u+\eta v)]d\xi d\eta \end{aligned} \tag{2.9}$$

In the case of $d = f$, The quadratic phase factor before transform integration vanishes. If the input is in the front focal plane to lens, the phase bending vanishes, and an accurate Fourier transform relationship is obtained. In conclusion, lensing allows for Fourier changes.

THE 4F SYSTEM

The 4F system refers to a lens system consisting of 2 lenses with a lens spacing that is the sum of the focal lengths of the two adjacent lenses. Furthermore, the composition shows that the 4F system consists of a cascade of two Fourier transforms. This feature enables the 4F system to perform the function of optical filtering. By introducing a spatial filter in the Fourier plane of the system, specific frequency components or spatial features in the output signal can be selectively removed or enhanced.

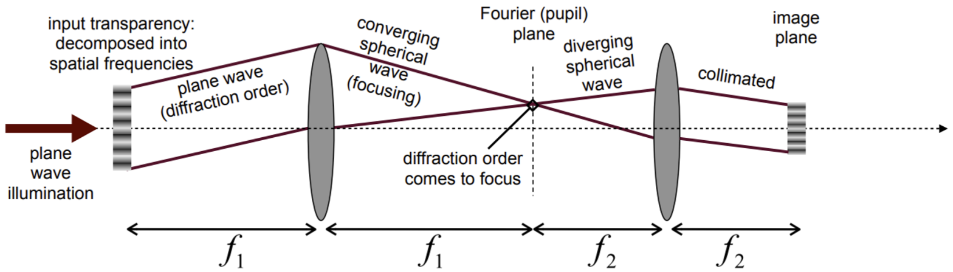

Figure 2.4: 4F system[25]

In figure2.4 depicts the grid configuration of the two 4f telescopes. The system consists of two lenses with focal lengths f1 and f2. The input is a diffractive planar illumination at a distance of f1 from the first lens. According to the Fourier transform theory of lenses in the previous section, we can obtain the Fourier transform of the planar illumination in the Fourier plane. In the Fourier plane, a filter can be inserted for spectral processing. Another lens is placed after another focal length, f2, which acts as a Fourier transform of the input-processed spectrum and outputs it in its post-phase plane. Note that the output of the image plane varies in size due to the different focal lengths of the two lenses and that this output is also inverted since two Fourier transforms are used in succession rather than one transform followed by an inverse transform.

The present work takes advantage of this to address the problem of zero-order diffraction, which will be described in subsequent section. In addition, the collimated light produced between the two lenses of the 4f telescope proves advantageous. It allows the strategic placement of optical elements, such as filters or dichroic mirrors, in this spatial plane without introducing significant phase changes.

In conclusion, this experiment can filter the structured light generated by SLM by the 4F system and find the proper position of the observation object and the lens. The SLM is typically used as the plane wave illumination in figure2.4, and the light incident on the SLM is modulated into a diffraction pattern of the desired pattern. Firstly, this will result in the desired structured illumination light pattern in the Fourier plane, and the object to be measured can be appropriately illuminated by placing it in the Fourier plane. Secondly, it is also possible to put a filter between the two lenses to filter out unwanted light. Finally, it is also possible to place another lens f_3 after the second lens, behind which the CCD can obtain an image in the Fourier plane, which is also the object illuminated by the structured illumination light. This will be described in detail in the experiment setup.

2.2.2. ZERO-ORDER SPOTS EFFECTS AND SOLUTIONS

Through Fourier Optics, we have analyzed the diffraction of SLM, lenses, and 4F systems. However, for SLM, which generates diffraction patterns, another problem will affect imaging quality in the imaging process: zero-order diffraction.

THEORY AND EFFECTS OF ZERO-ORDER DIFFRACTION

Diffraction order is a concept that arises when the incident light is reflected on a diffraction grating, which shows in figure2.5. Diffraction order is an integer value that satisfies the following diffraction grating equation:

$$m\lambda = d(sin\alpha + sin\beta) \tag{2.10}$$

Where m is an integer value describing is the diffraction order, λ is the wavelength of the light, d is the spacing between the diffraction cells on the grating, α is the angle of incidence of the light, and β is the angle of diffraction of the light leaving the grating.

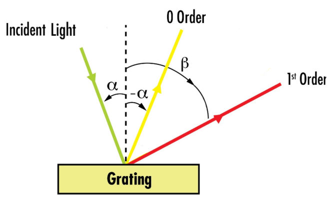

Figure 2.5: Diagram of 0 and 1st order diffraction

Zero-order diffraction occurs when the SLM converts the incident light signal into a diffraction pattern of the desired pattern and then obtains the desired pattern by Fourier transform.

In the case of SLMs, the diffraction efficiency is affected by small filling factors in the phase actuator and dead zones caused by imperfect permeability-enhancing membranes at the SLM front electrode. It allows a small portion of the incident beam to be unmodulated and produces an unmodulated beam that is focused by the lens into a zero-order spot[26]. Where fill factor means the ratio of the effective area to the total area of the aperture[27]. In conclusion, the zero-order diffraction is not containing any useful information[26].

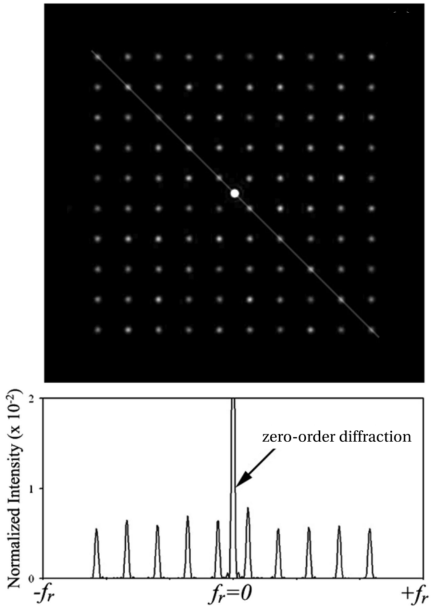

Figure 2.6: Zero-order diffraction schematic[28]

However, zero-order diffraction can affect imaging because the intensity of zero-order diffraction is extreme. It could be ten times stronger than each predetermined spot in the light pattern[28], as shown in figure2.6.

In a 4F system, diffraction of different orders will be represented as figure2.7. As stated in the previous section, we modulate the incident light into a diffraction pattern of SLM's desired structured illumination pattern obtained in the Fourier plane. So, the zero-order diffraction will be located in the middle of the structured illumination light pattern, and the first-order diffraction containing the information of this pattern will realize the structured illumination light pattern in the Fourier plane.

SOLUTIONS FOR ZERO-ORDER DIFFRACTION

Mask and linear shift Firstly, the optical path analysis enables us to obtain a way to shield zero-order diffraction. The schematic of the 4F system reveals that the simplest way to achieve shielding from zero-order diffraction is to place a mask in the Fourier plane, which is a high-pass filter.

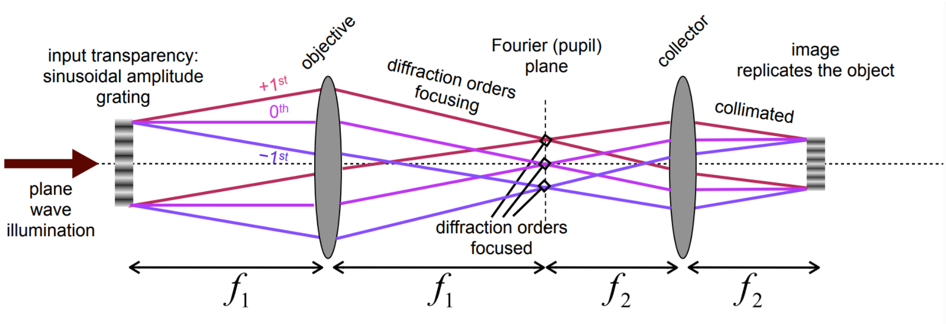

Figure 2.7: 4F system with diffraction order schematics[25]

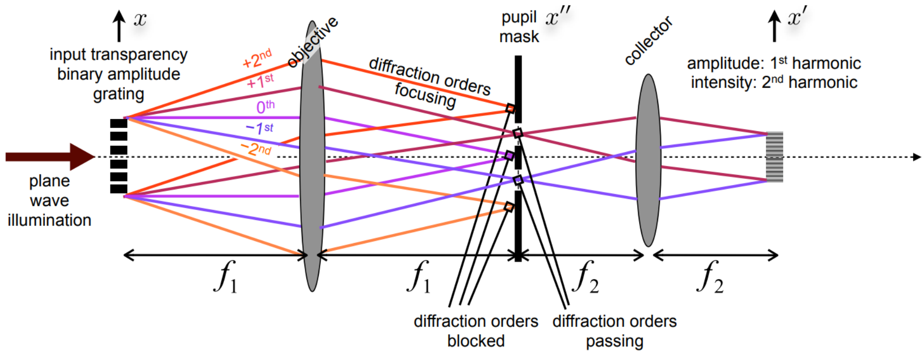

Figure 2.8: Diagram of blocking zero-order diffraction[25]

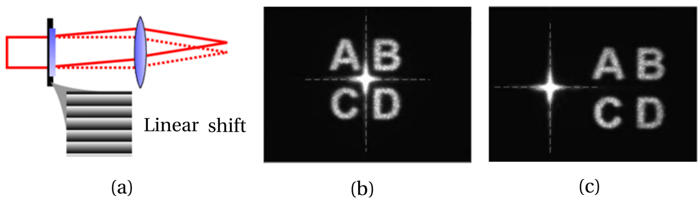

Figure 2.9: (a) Indicates the change in the optical path resulting from adding a linear phase shift to the SLM. (b) denotes the imaging of SLM after lens focusing without adding any shift, (c) denotes the imaging of SLM after lens focusing with the addition of linear phase-shift[29]

In addition, there is the treatment of zero-order diffraction using the SLM software. Adding a linear phase shift makes it possible to separate the distance between the zero-order diffraction and the first-order diffraction, thus reducing the effect of the zero-order diffraction. In the figure2.9(b), we can see that without the linear phase shift, the zero-order diffraction is located in the middle of the pattern as in the general case. With the addition of the linear phase shift, the image composed of the first-order diffraction containing information is separated from the zero-order diffraction, as shown in figure2.9(c).

2.3. EXPERIMENTAL DESIGN

2.3.1. EXPERIMENTAL EQUIPMENT

HOLOEYE PLUTO SLM

The spatial light modulator (SLM) used in our study was the Holoeye PLUTO NIR shown in Fig. (reffig:21.1), which belongs to the category of phase-only SLMs. PLUTO-2.1 phase-only SLM consists of a driver with a standard digital video interface, in particular HDMI (High-Definition Multimedia Interface), and a phase-only LCOS (Liquid Crystals on Silicon) micro-display. The microdisplay is connected to the driver unit via a flexible cable. The driver unit receives commands via standard DVI (Digital Video Interface) signals from the computer's graphics card. The driver unit uses an HDMI interface to control the phase function, while communication with the driver unit is via the USB interface. The SLM may be adjusted for various wavelengths via the USB interface by altering the voltage-to-gray level distribution (gamma control) and the dynamic range (voltage across the LC cell). The wavelength range of this SLM is 1400 - 1700 nm. The provided Pattern Generator program, the SLM Slideshow Player software, or standard image viewer software can all be used to address the SLM. Connection scheme shows in Figure2.11.

Figure 2.10: PLUTO phase modulator

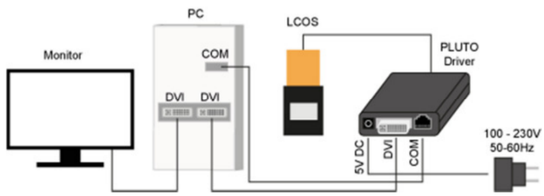

Figure 2.11: Connection scheme

Principle of phase modulation HOLOEYE's spatial light modulator (SLM) system is based on reflective liquid crystal microdisplays, specifically reflective LCOS (Liquid Crystal on Silicon) technology, as depicted in figure2.12. The LCOS microdisplay operates by applying a voltage to each pixel between the CMOS and transparent electrode layers.

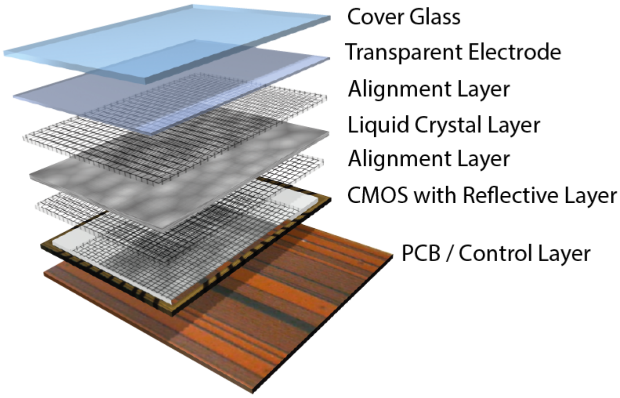

Figure 2.12: LCOS Structure and Materials

Liquid crystal (LC) material adoption in the SLM is motivated by its optical and electrical anisotropy. The LC material exhibits varying behavior based on the applied voltage, corresponding to specific gray levels within the LC cell. The electrical anisotropy gives rise to a LC Variable tilt of the molecules when subjected to the voltage, which shows in Figure2.13. Additionally, because of the optical anisotropy of LC molecules, this tilt changes the LC material's refractive index(for an appropriate incident polarization, depending on the device version). Consequently, the refractive index alteration affects the LC cell's optical path length.

The electrical anisotropy, which refers to the dipole property of the LC, enables the LC molecules to orient themselves variably in response to an applied electric field. On the other hand, optical anisotropy, also known as birefringence, indicates that the LC molecules possess different refractive indices: one for the normal molecular axis (no optical activity) and another for the particular molecular axis (exhibiting optical activity). The electrical and optical anisotropy combination allows for phase modulation in the LCOS microdisplay. In practical terms, the display undergoes processing with an 8-bit grayscale bitmap image, where each gray level corresponds to a specific average voltage applied to the LC layer of each pixel. The addressed gray levels are then translated into phase levels.

Calibration of SLM SLMs need to be calibrated before they can be used. This is due to errors on the SLM's LC layer that arise from phase correspondence in terms of control and spatial variations in the LC layer that would exist during the preparation process in

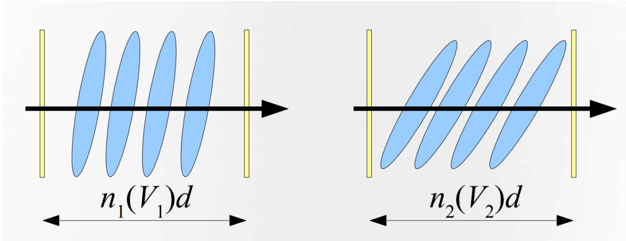

Figure 2.13: Holoeye PLUTO operating principles

terms of undesired optical flatness. Therefore, calibration is required for better control.

There are many ways to calibrate the SLM. Firstly interferometric methods[30], which include quantitative phase measurements using phase masks[31] or through interferometric microscopy[32]. Secondly, calibration using digital holography[33]. Additionally, it can also be calibrated through a gamma curve.

The Holoeye PLUTO NIR phase-only SLM manual recommends calibrating the SLM using a gamma curve. By calibrating the SLM, it is possible to improve diffraction efficiency. The changing of geo-metrical settings can be used to modify brightness, contrast and electro-optical response through the use of a new gamma curve in order to bridge the error on the LC layer. The gamma curve used by the modulator is the table of data that makes up this curve: the gamma table. When using the PLUTO phase modulator, this can be displayed via the Holoeye software. This is usually used to perform gamma correction and black-and-white balance adjustments. The gamma table can then be stored on and reloaded from the disk, and other gamma tables can also be loaded. The length of the gamma table in the PLUTO SLM is 1024 different codes. Although the input signal is only encoded in 8 bits, the correction circuitry inside the driver chip uses the additional codes (half and quarter grey steps). The phase response is defined by values 1,5, 1021. the control elements on the digital potentiometers tab can set the black and white voltage of the LC display via digital variable. The control elements on the digital potentiometers tab can set the black-and-white voltage of the LC display via digital variable resistors (DVRs) to adapt the SLM dynamic range.

Resolution of SLM The resolution of the illumination pattern is also crucial in structured illumination. Further, the resolution of the structured illumination pattern is determined by the resolution of the SLM. So we need to analyze the resolution of the SLM.

Let us first make assumptions about the use of SLM. Firstly if the SLM is imaged directly at a distance z, then according to equatio2.5, what we get in the image plane is the Fourier transform of the SLM with the exact resolution as or proportional to the liquid crystal layer of the SLM.

Secondly, let us first assume a simple scenario: there is a lens in front of the SLM, which is one lens focal length away from the SLM and imaged at the lens focal length. Then we can assume that the size of a pixel point at the SLM is $\Delta x and y$ and the size of this pixel point at the image plane is $\Delta u and \Delta v$. According to equation2.9, we can obtain the following equation:

$$U_f(\Delta u, \Delta v) \propto \frac{1}{\lambda f} F_o(\frac{\Delta u}{\lambda f}, \frac{\Delta v}{\lambda f}) \tag{2.11}$$

So, we can obtain the resolution of the SLM with a lens[34]:

$$\Delta u \times \Delta v = \frac{\lambda f}{N_u \Delta x} \times \frac{\lambda f}{N_v \Delta y} \tag{2.12}$$

where $N_u \times N_v$ are the number of discrete points in the image plane

Diffractive optical element(DOE) phase function

The SLM can achieve a diffractive pattern by calculating the required image's diffractive optical element (DOE) image. Calculation of the diffractive optical element (DOE) image of the desired image is achieved by the iterative Fourier transform algorithm (IFTA).

The Iterative Fourier Transform Algorithm (IFTA) generates pure phase holograms. This method is characterized by the iterative transfer of the Fourier transform in two planes to get the information about the phase of the light field in the plane of the hologram. The final output of the IFTA is the phase spectrum of the desired target in the spectral domain, i.e., the DOE phase function, and the phase function of the calculated diffraction pattern is displayed on the SLM.

SANTEC TUNABLE LASERS

The laser chosen for this study is the Santec tunable laser TSL-550, as shown in figure 2.14. A high-performance tunable laser, the TSL-550 combines high power and an excellent signal-to-noise ratio in its output. It also has a large tuning range. It maintains a high output power of over +10 dBm while having a high signal-to-noise ratio of over 90 dB/0.1 nm. It achieves an output power of up to 10dBm at the required wavelength of 1550nm. In addition, the light output from this laser is also polarized horizontally, as required for SLM.

1951 USAF RESOLUTION TEST TARGETS

Thorlabs offers positive and negative 3"x3"(76.2mmx76.2mm) resolution test targets which show in figure2.15. It are created by chrome plating a soda lime glass foundation. The 3"x3" targets give a maximum resolution of 228.0 line pairs (one light line and one dark line) per millimeter and contain 10 groups (-2 to +7) with 6 elements each. These targets include three-line feature sets, which reduce the chance of spurious resolution and assist in preventing false resolution measurements.

Figure 2.14: Santec tunable lasers TSL-550

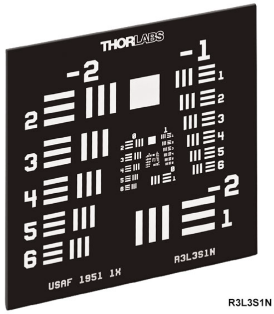

Figure 2.15: 1951 USAF Resolution Test Targets

CHARGE COUPLED DEVICE(CCD) CAMERA

Figure 2.16: CCD camera

This experiment uses a CCD camera to image the structured light illumination pattern and also uses this to image the resolution chart imaging by the structured illumination.

The XEVA 320 SERIES CCD camera was selected for this paper, which shows in figure2.16. The resolution of this camera is 320×256. The size of each pixel pitch is $30\mu m$. The Spectral range of the camera is between 900 - 1700 nm, the laser used in this experiment is 1550 nm, which is within the observation range of the camera.

2.3.2. OVERALL EXPLANATION OF SETUP

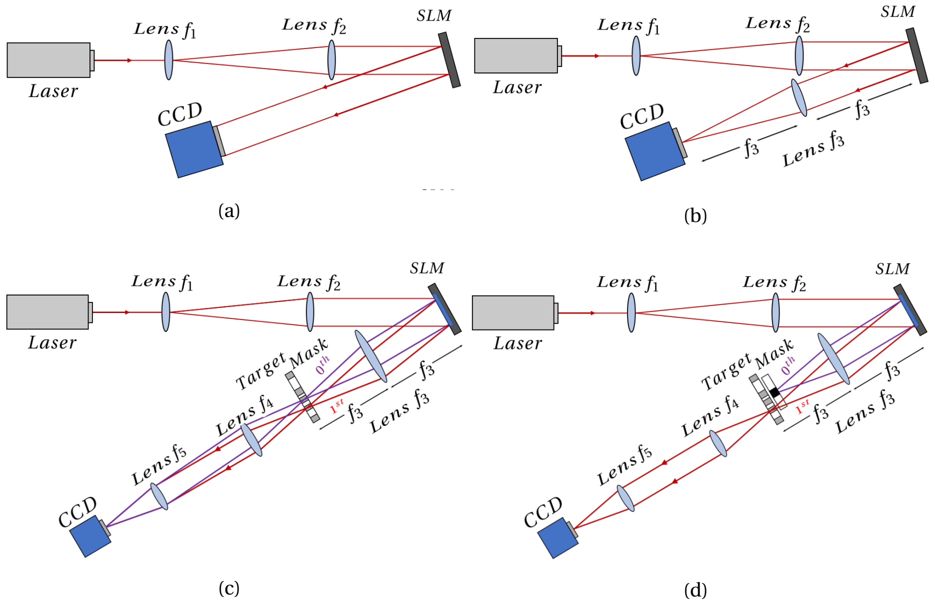

Figure 2.17: Figure (a), (b), (c), and (d) shows the four experimental setups used in this paper, among which experimental setup (A) and experimental setup (B) can be used to study the imaging modality of SLM. Moreover, experiment setup (C) solves the stable mapping of structured illumination light from the Fourier plane to the camera. Experiment setup (D) is used to solve the zero-level diffraction problem.

The goal is to investigate how to achieve structured illumination light by SLM. So the first thing to investigate is the best illumination method for SLM. Secondly, the problems in the process of realizing structured illumination light by SLM need to be solved, such as the zero-level diffraction problem. Finally, stable mapping from structured illumination to the camera has to be achieved. The different experimental setups are shown in figure2.17.

There are a total of four experimental setups for this experiment, which are shown in figure2.17. We refer to these four experimental setups by experiment setup (A), (B), (C), and (D) in this and subsequent sections. The focal lengths of the lenses used for the experimental setup are as follows. The focal length of lens f_1 is $f_1 = 30mm$. The focal length of lens f_2 is $f_2 = 150mm$. The focal length of lens f_3 is $f_3 = 200mm$. The focal length of lens f_4 is $f_4 = 100mm$. The focal length of lens f_5 is $f_5 = 75mm$. In addition, the focal length of f_3 in figure2.17(b) is 100mm.

The composition of experiment setup (A) is shown in figure2.17(a). Light with a wavelength of 1550 nm is emitted from the laser and illuminated onto the first lens through a collimator. The second lens has a larger focal length than the first lens, so it spreads the beam so that the laser beam completely fills the SLM screen. The camera takes a direct picture of the laser beam after reflection from the SLM, which is tilted at an angle of about 10 degrees.

This setup (A) has two purposes. The first is to study the effect of Fraunhofer diffraction on the structured illumination pattern during SLM imaging. The second purpose is to study the illumination pattern formed by the SLM without DOE calculations and its SIM imaging.

The composition of experiment setup (B) is shown in figure2.17(b). Setup (B) is the same as Setup (A) before SLM. However, after the SLM reflects the laser, lens 3 is placed at a focal distance from the lens 3, the laser passes through the lens 3, and then the camera is placed at a focal distance from the lens 3. At this time, the camera is located in the Fourier plane.

The purpose of this experimental setup (B) is to investigate the effect of the Fourier transform on the structured illumination pattern of the SLM in the Fraunhofer diffraction state under the influence of a single lens and to compare the results of this experimental setup with the lensless experimental setup in order to select a more appropriate Fourier transformation of the diffraction pattern.

The composition of experiment setup (C) is shown in figure2.17(c). Setup (C) before SLM is the same as setup (A). After reflecting the laser at the SLM, the structured illumination is first Fourier transformed through the first lens, with the desired imaging target located in the Fourier plane. After that, lens 4 is placed at the focal length of one lens 4. After the laser light passes through lens 4, lens 5 is placed at the focal length of one lens 4 plus lens 5. The camera is placed at the focal length of one lens 5 after the lens 5. In addition, the propagation of zero-order diffraction is shown in purple; first-order diffraction is shown in red. We can see that the zero-order diffraction affects the imaging, so we need the next experimental setup to improve it.

The composition of experiment setup (D) is shown in figure2.17(d). It is the setup for the structured illumination pattern with DOE calculations. Compared to the previous experimental setup, this setup adds a mask in front of the target. This allows the information at the target to be accurately transmitted to the camera through the two lenses behind the target while also eliminating the interference of zero-order diffraction.

2.4. RESULT

This section presents the results of the generated structured illumination patterns with the various setups. There are 2 experiments in this section. The first experiment aimed to obtain the optimal method for achieving structured illumination of light by diffraction. The purpose of the second experiment is to compare the difference between the structured illumination patterns obtained by the experimental setup that can stably get structured illumination patterns.

SLM ACHIEVING STRUCTURED ILLUMINATION BY DIFFRACTION

The principle of SLM diffraction imaging by diffraction is that the incident light is modulated into a diffraction pattern of the desired illumination pattern by SLM. Then Fourier transformed to obtain desired illumination pattern. Furthermore, in the chapter Fourier optics part, we get the equations2.5 and 2.9, which shows that on the one hand, at the distance of the Fraunhofer diffraction, we can obtain a Fourier transform in equation 2.5. On the other hand, a lens can also provide a Fourier transform in equation 2.9. Thus we get the structured illumination pattern obtained by Fourier variation generated by distance and the structured illumination light pattern obtained by Fourier transform generated by lens by setup(A) and setup(B), respectively.

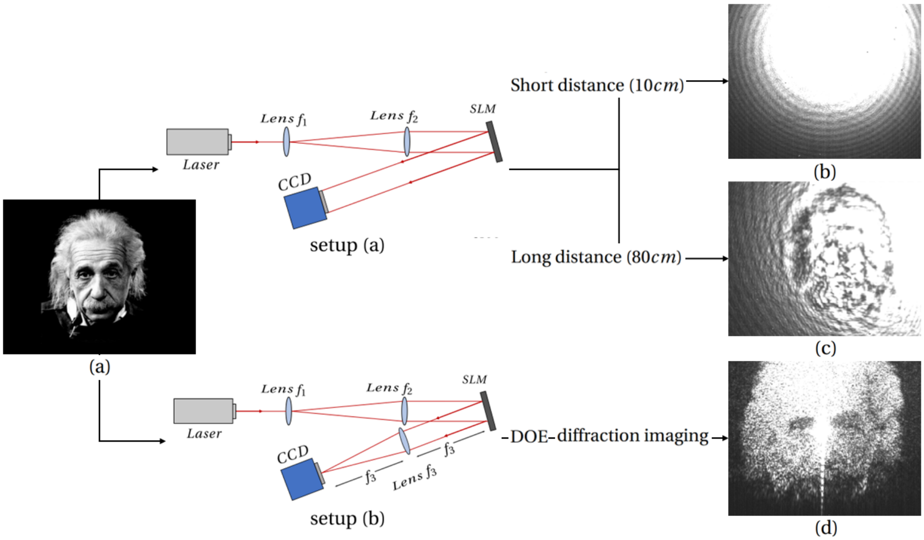

Figure 2.18: Figures (b)-(d) show the laser being modulated by SLM to produce the shown in diagram (a). Figure (b) shows the camera's imaging of the SLM-modulated structured light pattern without adding a lens. Figure (c) shows the imaging of the structured light pattern using the camera at a distance of 80cm from the SLM. Figure (d) shows the camera imaging of the SLM-modulated structured light pattern after a lens with a focal length of 100mm

During the experiment, we make the structured illumination pattern obtained by the final camera as Einstein's head by setup(A) and setup(B). We can see that Fraunhofer diffraction can achieve the Fourier change when the distance $z \geq \frac{2a^2}{\lambda} = 82.6 \times 10^{-6} m$. However, due to the unevenness of the surface of the SLM LCD diffraction will also be imaged, and the zero-order diffraction effect of this method is huge, so it does not get good imaging, as shown in figure2.18(b). However, when the Fourier transform is achieved through distance, the distance simultaneously generates wave perturbations that cause a degradation in the quality of the illumination pattern, as shown in figure2.18(c). On the other hand, the lens implementation of the Fourier transform gives a sharper illumination pattern with a smaller experimental setup, as shown in figure2.18(d).

In conclusion, if the SLM is needed for diffraction to achieve a structured illumination light pattern, obtaining the Fourier variation through a lens is a better approach.

STRUCTURED ILLUMINATION PATTERNS REALIZATION

There are two ways to achieve structural illumination light patterns through SLM. One is mentioned in the previous experiment, by modulating the incident light into a diffraction pattern, as shown in the figure2.19(b). The other method modulates the incident light into the desired structural illumination pattern. Furthermore, the pattern presented on the SLM is the desired illumination pattern, and the incident light will reflect the illumination pattern when injected into it, as shown in the figure2.19(a).

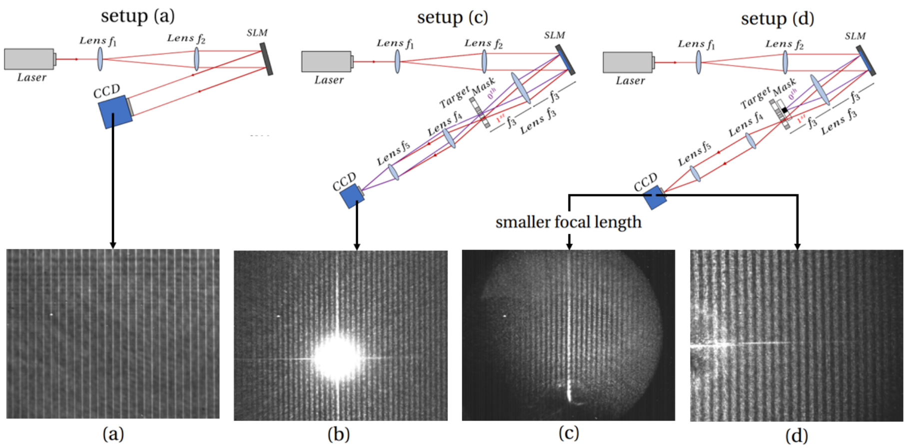

Figure 2.19: Figures (a)-(c) show the structural illumination patterns imaged by the camera under different experimental setups. The experimental setup in Figure (a) does not add any lenses after SLM, and DOE modulation is not used. The experimental setup used in Figure (b) has three lenses added after SLM. Figure (c) shows the illumination pattern imaged with the addition of blocking and phase shift. Figure (d) uses a lens set with a smaller magnification ratio, and the third lens after the SLM has been chosen to have a smaller focal length

As a conclusion, by comparing2.19(a) and 2.19(b). Direct modulation of incident light 2.19(a) has the advantage that the structural illumination pattern will propagate steadily along the optical path and will not give rise to the problem of zero-order diffraction. However, the disadvantages are that the contrast is not high, and the background noise is relatively high. The background noise comes from the fact that the light reflected by the SLM is diffracted as it travels over a certain distance, resulting in noise.

Modulation of incident light by diffraction2.19(b) has the advantage of higher contrast and no background noise. However, the problem of zero-order diffraction arises, and the required illumination pattern only appears in the Fourier plane. Thus, two problems need to be solved: one is to exclude zero-order diffraction in the illumination pattern, and the other is to project the illumination pattern in the Fourier plane to the camera. The solution to zero-order diffraction is discussed in the previous section on zero-order diffraction, which can be reduced by placing a mask in front of the Fourier plane to block the zero-order diffracted light points and by adding a linear phase to separate the zero-order diffraction from the first-order diffraction. The final illumination pattern after troubleshooting the problem is shown in figure2.19(c) and (d). The difference between these two results is that the magnification ratios are different. While too small a magnification ratio achieves finer stripes, it also creates out-of-focus areas in the periphery.

It is worth noting that the illumination pattern still has the effect of zero-order diffraction after masking the zero-order diffraction mask. This shows that although masking is a simple method, there is still room for improvement. It is a method worth exploring through algorithms directly on the SLM. An idea for improvement could be by intercepting the part of the camera's view that is not affected by zero-order diffraction. The images in this study are all in the maximum field of view of the camera, so the method of intercepting a part of the view is possible. However, as can be seen in figure2.19(d), the intensity of the illumination pattern that is not affected by zero-order diffraction is decaying and is not uniform, so the view that can be used is limited. So finding a uniform illumination pattern is a requirement for using this method.

Effect of rotating lens The rotating lens can also separate first-order diffraction from zero-order diffraction. Taking figure 2.7 as an example, assuming that we rotate the lens 2, then the separation of the zero-order diffraction and the first-order diffraction will also have a small increase, which is also verified in the experiment. However, while separating the first-order diffraction from the zero-order diffraction, the illumination pattern imaged by the diffraction will also be distorted by the rotation of the lens. Therefore, the following experimental studies do not take the approach of rotating the lens.

3

STRUCTURED ILLUMINATION IMAGING REALISATION

This chapter focuses on the realisation of structural illumination imaging. The principle of structural illumination imaging is introduced in the first section. Moreover, the algorithm for implementing structural illumination imaging is introduced. In the last section, the effects of the experimental setup, illumination frequency and angle on imaging are analysed according to the experimental results.

3.1. PRINCIPLE OF STRUCTURAL ILLUMINATION IMAGING

The principle of SR-SIM can be explained in the frequency domain. Microscopes have a specific range of observation or spatial bandwidth when observing objects. This bandwidth also has a cut-off frequency, which generally depends on the microscope's numerical aperture (NA) and illumination wavelength (λ), which shows in Figure3.2.

$$Cut-offFrequency(K_c(f)) = 2NA/\lambda \tag{3.1}$$

Consider an object x illuminated by a sinusoidal illumination pattern p with periodicity k_0, as shown in figure3.1(a). The objective forms an image f. We assume that r is the coordinate vector. $\otimes$ is convolution.

$$f(r) = (x(r) \cdot p(r)) \otimes h(r) \tag{3.2}$$

Let $F, X, PandH$ be the Fourier transforms of the functions f, x, p and h. H is the optical-transfer function (OTF) of the system, and h is the point spread function (PSF) of the system.

$$F(k) = (X(k) \otimes P(k)) \cdot H(k) \tag{3.3}$$

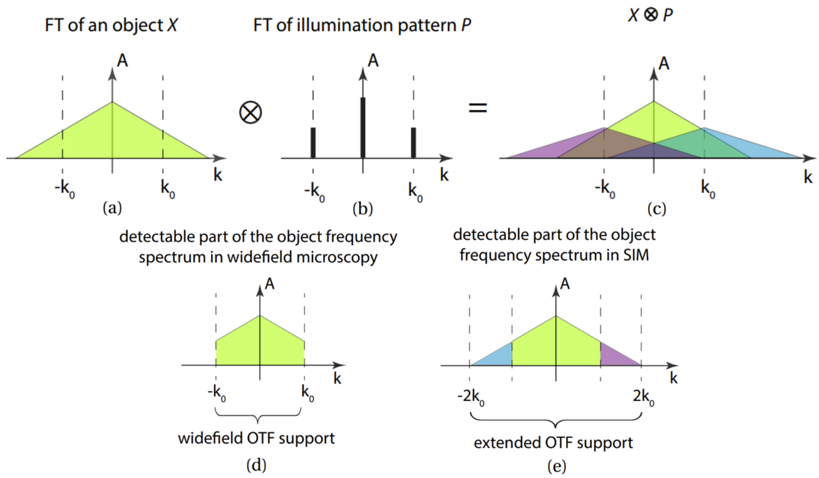

Figure 3.1: Structured illumination principle.Figure (a), (b) and (c) represent the spatial spectral convolution of the object and illumination modes resulting in three regions in the spatial spectrum. Previously unobserved portions of the object spectrum are shifted into the passbands of the microscope OTF. (d) denotes the frequency-domain space that the microscope can observe, and (e) denotes the frequency-domain space that can be observed by the SLM method, which in this case is the complete spectrum of the object.[35]

To simplify the model, we assume that $k_0 = k_c$. k_0 is the frequency of structured illumination. The result obtained by convolution is shown in the figure3.1(c). We assume that ϕ is the phase of the illumination pattern and the illumination pattern is sinusoidal. The mixture of three spectral components, imaged by the microscope, is:

$$F(k) = (X(k) + \frac{1}{2}X(k-k_0)e^{2\pi i\phi} + \frac{1}{2}X(k-k_0)e^{-2\pi i\phi}) \cdot H(k) \tag{3.4}$$

The previously undetectable parts of an object's spatial frequency spectrum ($k \in [k_0, 2k_0]$ and $k \in [-2k_0, -k_0]$) move into the transmission pass-band and could now be detected because two of these frequency spectra are moved by k_0. Therefore, SIM is used as a wide field microscope, which shows in figure3.1(e).

On the other hand, when the periodicity of the illumination pattern k_0 is less than k_c, then the frequency domain spatial information that can be observed is $k \in [-k_0 - k_c, k_0 + k_c]$, and less frequency domain information is obtained. If when k_0 is greater than k_c, the frequency domain spatial information that can be observed is $k \in [-k_0 - k_c, k_0 + k_c]$ if the range of the object's frequency domain information is greater than k_c. In conclusion, the higher the frequency of the illumination pattern, the more frequency domain information can be observed. Thus the higher the quality of the imaging will be.

Let us expand this to the two-dimensional plane. The frequency domain has two components, k_x and k_y. Assuming a microscope with a Kc imaging system cut-off frequency, then the spectrum of spatial frequency that the imaging system can shown is in figure3.2. (b). In figure3.2. (c), the middle grph represents the frequency spectrum that was detected under uniform light, and the left and right terms, which are denoted by +Ko and −Ko, respectively, indicate the frequency spectrum that was shifted under structured illumination[1]. Overlaying the two spectra reveals that the frequencies that can be resolved extend from Kc to Kc+Ko.

Moreover, when the illumination pattern is tilted, it will have k_x and k_y in the frequency domain. As shown in figure3.2(e), SIM then allows more frequency domain information to be observed at the two-dimensional level. It is also concluded that the more angles of tilt, the wider the range that can be observed in the frequency domain and the higher the image quality obtained.

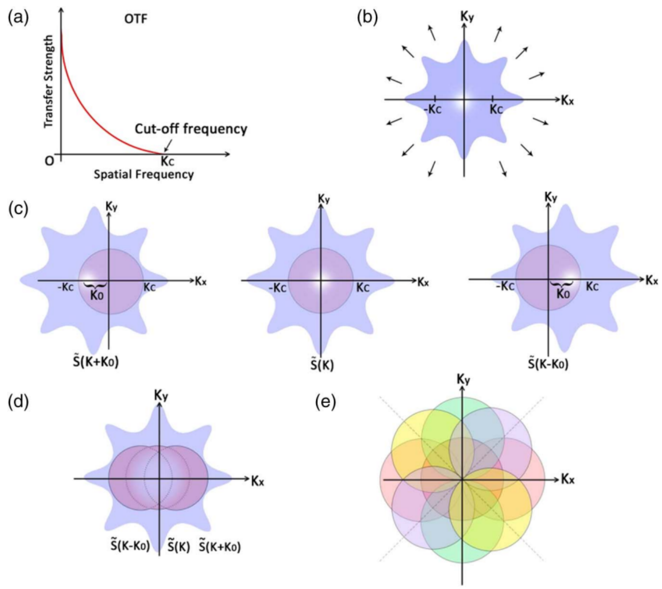

Figure 3.2: Structured illumination principle. Figure (a) represents the cutoff frequency of the microscope, (b) represents the frequency domain space, and (c) represents the change in the frequency domain space that can be observed due to the change in the illumination pattern. Figures (d) and (e) represent the expansion of the frequency domain space obtained by imaging through structured illumination.[1]

3.2. STRUCTURAL ILLUMINATION IMAGING ALGORITHM

We reconstruct the images by using Matlab code. The principle of the reconstruction code is described below. The flowchart of the reconstruction algorithm is shown in figure3.3. The following is an example of nine structural illumination image reconstructions.

Take the example of SIM, where the structural illumination pattern P_θ is sinusoidal. The

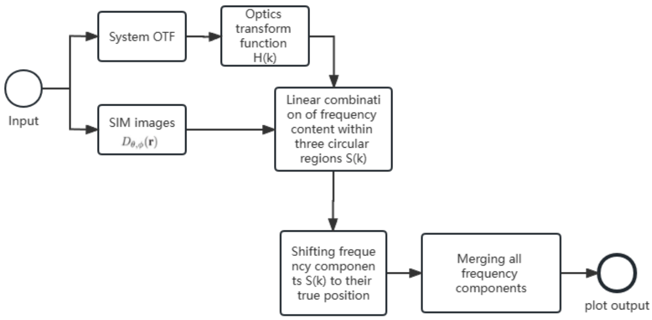

Figure 3.3: Flowchart of the reconstruction algorithm

rotation angle of the illumination pattern is θ, and the phase is ϕ.

$$P_{\theta,\phi(\mathbf{r})} = -\cos\left(2\pi\mathbf{p}_\theta\cdot\mathbf{r}+\phi\right) \tag{3.5}$$

The inputs to the reconstruction algorithm are nine SIM images $D_{\theta,\phi(\mathbf{r})}$, corresponding to three different rotation angles $\theta = \theta_1, \theta_2, \theta_3$, and three different phase $\phi = \phi_1, \phi_2, \phi_3$. Also, the OTF of the system and the frequency $\mathbf{p}_\theta$ of the illumination pattern need to be given as an input to the algoritm.

Let $I_{\theta,\phi}(\mathbf{r})$ be the illumination sinusoidal intensity pattern and $S(\mathbf{r})$ be the density distribution inside the specimen.

$$I_{\theta,\phi}(\mathbf{r}) = I_o\left[1-\frac{m}{2}\cos\left(2\pi\mathbf{p}_\theta\cdot\mathbf{r}+\phi\right)\right] \tag{3.6}$$

Where $r(x,y)$ is the (two-dimensional) spatial position vector, I_o is the maximum illumination intensity, and m is the modulation factor. The (sinusoidal) illumination frequency vector is $\mathbf{p}_\theta = (cos\theta, sin\theta)$. According to equation3.3, we can get that:

$$\tilde{D}_{\theta,\phi}(\mathbf{k}) = \left[\tilde{I}_{\theta,\phi}(\mathbf{k})\otimes\tilde{S}(\mathbf{k})\right]\cdot\tilde{H}(\mathbf{k})+\tilde{N}(\mathbf{k}) \tag{3.7}$$

where $\tilde{H}(\mathbf{r})$ is optical system's OTF, and $\tilde{N}(\mathbf{r})$ is noise. $\tilde{D}_{\theta,\phi}(\mathbf{k})$ is a linear combination of frequency content within three circular regions of specimen $\tilde{S}(\mathbf{k})$, and also is Fourier transform of $D_{\theta,\phi(\mathbf{r})}$. where $I_o/2$ is a constant representing the intensity and is scale of the image, so it can be assumed to be 1 to simplify the problem.. By bringing in equation3.6 and transforming, it can be obtained[36]:

$$\begin{bmatrix} \tilde{D}_{\theta,\phi_1}(\mathbf{k}) \\ \tilde{D}_{\theta,\phi_2}(\mathbf{k}) \\ \tilde{D}_{\theta,\phi_3}(\mathbf{k}) \end{bmatrix} = \frac{I_o}{2}\mathbf{M}\begin{bmatrix} \tilde{S}(\mathbf{k})\tilde{H}(\mathbf{k}) \\ \tilde{S}(\mathbf{k}-\mathbf{p}_\theta)\tilde{H}(\mathbf{k}) \\ \tilde{S}(\mathbf{k}+\mathbf{p}_\theta)\tilde{H}(\mathbf{k}) \end{bmatrix} + \begin{bmatrix} \tilde{N}_{\theta,\phi_1}(\mathbf{k}) \\ \tilde{N}_{\theta,\phi_2}(\mathbf{k}) \\ \tilde{N}_{\theta,\phi_3}(\mathbf{k}) \end{bmatrix} \tag{3.8}$$

$$\begin{bmatrix} \tilde{S}(\mathbf{k})\tilde{H}(\mathbf{k}) \\ \tilde{S}(\mathbf{k}-\mathbf{p}_\theta)\tilde{H}(\mathbf{k}) \\ \tilde{S}(\mathbf{k}+\mathbf{p}_\theta)\tilde{H}(\mathbf{k}) \end{bmatrix} = \mathbf{M}^{-1} \begin{bmatrix} \tilde{D}_{\theta,\phi_1}(\mathbf{k}) \\ \tilde{D}_{\theta,\phi_2}(\mathbf{k}) \\ \tilde{D}_{\theta,\phi_3}(\mathbf{k}) \end{bmatrix}. \tag{3.9}$$

$$\mathbf{M} = \begin{bmatrix} 1 & -\frac{m}{2}e^{-i\phi_1} & -\frac{m}{2}e^{+i\phi_1} \\ 1 & -\frac{m}{2}e^{-i\phi_2} & -\frac{m}{2}e^{+i\phi_2} \\ 1 & -\frac{m}{2}e^{-i\phi_3} & -\frac{m}{2}e^{+i\phi_3} \end{bmatrix}. \tag{3.10}$$

When m = 1, we can get $\tilde{S}(\mathbf{k})\tilde{H}(\mathbf{k}), \tilde{S}(\mathbf{k}-\mathbf{p}_\theta)\tilde{H}(\mathbf{k}), and \tilde{S}(\mathbf{k}+\mathbf{p}_\theta)\tilde{H}(\mathbf{k})$. These three quantities are reconstructed in the frequency domain so that we can obtain more information, which shown in figure3.4.

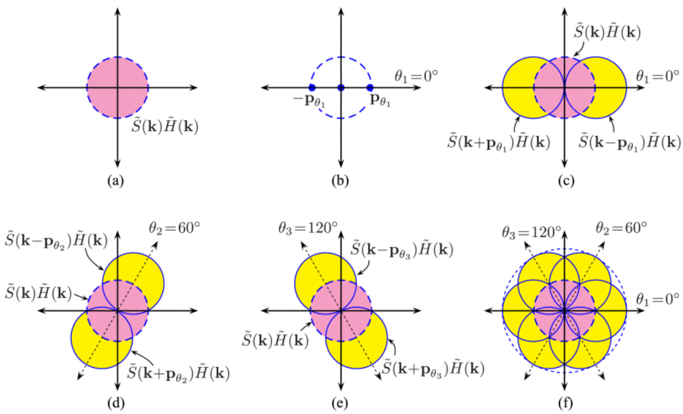

Figure 3.4: Principles of Structured Illumination Algorithm[36]

Assuming that $\Psi_{o,\theta}, \Psi_{p,\theta}, \Psi_{q,\theta}$ are average noise powers in $\tilde{S}(\mathbf{k})\tilde{H}(\mathbf{k}), \tilde{S}(\mathbf{k}-\mathbf{p}_\theta)\tilde{H}(\mathbf{k}), and \tilde{S}(\mathbf{k}+\mathbf{p}_\theta)\tilde{H}(\mathbf{k})$ and $\mathscr{A}$ and α are constants. Additionally, it is assumed that[36]:

$$\tilde{S}(\mathbf{k})\tilde{H}(\mathbf{k}) = m^2|\tilde{H}(\mathbf{k})|^2\mathscr{A}^2|\mathbf{k}|^{-2\alpha} + \Psi_{o,\theta} \tag{3.11}$$

We can see that there is a noise term in Equation 3.7, so the Wiener Filter is used for optimization. The $*$ in the upper right corner is the concomitant matrix. We define the frequency components after filtering as represented below[36]:

$$\tilde{S}_u(\mathbf{k}) = \left[\frac{\tilde{H}^*(\mathbf{k})}{|\tilde{H}(\mathbf{k})|^2 + \frac{\Psi_{o,\theta}}{\mathscr{A}^2|\mathbf{k}|^{-2\alpha}}}\right]\tilde{S}(\mathbf{k})\tilde{H}(\mathbf{k}) \tag{3.12}$$

$$\tilde{S}_u(\mathbf{k}-\mathbf{p}_\theta) = \frac{1}{m}\left[\frac{\tilde{H}^*(\mathbf{k})}{|\tilde{H}(\mathbf{k})|^2 + \frac{\Psi_{p,\theta}}{m^2\mathscr{A}^2|\mathbf{k}-\mathbf{p}_\theta|^{-2\alpha}}}\right] \tilde{S}(\mathbf{k}-\mathbf{p}_\theta)\tilde{H}(\mathbf{k}) \tag{3.13}$$

$$\tilde{S}_u(\mathbf{k}+\mathbf{p}_\theta) = \frac{1}{m}\left[\frac{\tilde{H}^*(\mathbf{k})}{|\tilde{H}(\mathbf{k})|^2 + \frac{\Psi_{q,\theta}}{m^2\mathscr{A}^2|\mathbf{k}+\mathbf{p}_\theta|^{-2\alpha}}}\right] \tilde{S}(\mathbf{k}+\mathbf{p}_\theta)\tilde{H}(\mathbf{k}). \tag{3.14}$$

The true locations of the frequency components $\tilde{S}(\mathbf{k}-\mathbf{p}_\theta)$ and $\tilde{S}(\mathbf{k}+\mathbf{p}_\theta)$ are centered respectively at frequencies p_θ and $-p_\theta$ in the frequency domain, see figure3.4. By employing Fourier shift theorem, frequency components $\tilde{S}(\mathbf{k}-\mathbf{p}_\theta)$ and $\tilde{S}(\mathbf{k}+\mathbf{p}_\theta)$ may be shifted to their true positions, to obtain their shifted variants (say) $\tilde{S}_s(\mathbf{k}-\mathbf{p}_\theta)$ and $\tilde{S}_s(\mathbf{k}+\mathbf{p}_\theta)$, respectively.

$$\mathscr{F}\left[\mathscr{F}^{-1}\left\{\tilde{S}_u(\mathbf{k}-\mathbf{p}_\theta)\right\} \times e^{-i2\pi(\mathbf{p}_\theta\cdot\mathbf{r})}\right] = \tilde{S}_s(\mathbf{k}-\mathbf{p}_\theta) \tag{3.15}$$

$$\mathscr{F}\left[\mathscr{F}^{-1}\left\{\tilde{S}_u(\mathbf{k}+\mathbf{p}_\theta)\right\} \times e^{+i2\pi(\mathbf{p}_\theta\cdot\mathbf{r})}\right] = \tilde{S}_s(\mathbf{k}+\mathbf{p}_\theta). \tag{3.16}$$

According to the convolution theorem we have

$$\tilde{D}_{SIM}(\mathbf{k}) = \left[\tilde{S}(\mathbf{k}) + \frac{m}{2}\tilde{S}_s(\mathbf{k}-\mathbf{p}_\theta)e^{-i\phi} + \frac{m}{2}\tilde{S}_s(\mathbf{k}+\mathbf{p}_\theta)e^{i\phi}\right]\cdot\tilde{H}(\mathbf{k}) + \tilde{N}(\mathbf{k})$$

According to the generalized Wiener filter approximation, we can combine all frequency components and get the final result D_{SIM}[36]:

$$\begin{aligned}\tilde{D}_{\mathrm{SIM}}(\mathbf{k}) = \sum_{\theta=\theta_1}^{\theta_3}\Bigg[&\left(\frac{\mathscr{A}^2|\mathbf{k}|^{-2\alpha}|\tilde{H}(\mathbf{k})|^2/\Psi_{o,\theta}}{w+\Omega(\mathbf{k})}\right)\tilde{S}_u(\mathbf{k})\\
&+\left(\frac{m^2\mathscr{A}^2|\mathbf{k}-\mathbf{p}_\theta|^{-2\alpha}|\tilde{H}(\mathbf{k}+\mathbf{p}_\theta)|^2/\Psi_{p,\theta}}{w+\Omega(\mathbf{k})}\right)\tilde{S}_s(\mathbf{k}-\mathbf{p}_\theta)\\
&+\left(\frac{m^2\mathscr{A}^2|\mathbf{k}+\mathbf{p}_\theta|^{-2\alpha}|\tilde{H}(\mathbf{k}-\mathbf{p}_\theta)|^2/\Psi_{q,\theta}}{w+\Omega(\mathbf{k})}\right)\tilde{S}_s(\mathbf{k}+\mathbf{p}_\theta)\Bigg]\end{aligned} \tag{3.17}$$

where

$$\Omega(\mathbf{k}) = \sum_{\theta=\theta_1}^{\theta_3} \left[\frac{\mathscr{A}^2|\mathbf{k}|^{-2\alpha}|\tilde{H}(\mathbf{k})|^2}{\Psi_{o,\theta}} + \frac{m^2\mathscr{A}^2|\mathbf{k}-\mathbf{p}_\theta|^{-2\alpha}|\tilde{H}(\mathbf{k}+\mathbf{p}_\theta)|^2}{\Psi_{p,\theta}} + \frac{m^2\mathscr{A}^2|\mathbf{k}+\mathbf{p}_\theta|^{-2\alpha}|\tilde{H}(\mathbf{k}-\mathbf{p}_\theta)|^2}{\Psi_{q,\theta}} \right] \tag{3.18}$$

and w is a constant, whose value is empirically adjusted to produce visibly optimum super-resolved image $D_{\text{SIM}}(\mathbf{r}) = F^{-1}[\tilde{D}_{\text{SIM}}(\mathbf{k})]$.

APPROXIMATION OF THE GENERALIZED WIENER FILTER

The conventional Wiener Filter estimate for $\tilde{S}_i(\mathbf{k})$ can be obtained[36]:

$$\tilde{S}_{o,i}(\mathbf{k}) = \left[\frac{|\tilde{H}_i(\mathbf{k})|^2}{|\tilde{H}_i(\mathbf{k})|^2 + \Psi_i/\Phi_i(\mathbf{k})} \right] \tilde{S}_i(\mathbf{k}). \tag{3.19}$$

The approximation of generalised Wiener Filter can be expressed as[36]:

$$\tilde{S}_a(\mathbf{k}) = \sum_{i=1}^{n} \left[\frac{\Phi_i(\mathbf{k})|\tilde{H}_i(\mathbf{k})|^2/\Psi_i}{w + \sum_{i=1}^{n} \Phi_i(\mathbf{k})|\tilde{H}_i(\mathbf{k})|^2/\Psi_i} \right] \tilde{S}_{o,i}(\mathbf{k}). \tag{3.20}$$

Where n is the number of image.

3.3. EXPERIMENTS AND RESULTS

This section presents imaging of resolution targets by structural illumination to study the effect of different experiment setup on the image quality., and to discuss the factors that affect imaging by structural illumination microscopy.

3.3.1. EFFECT OF EXPERIMENTAL SETUP

EXPERIMENTAL METHODS

In Chapter 2 on structured illumination pattern implementation, we described experimental setup (A) and (D), which are shown in figure2.17 for implementing structured illumination. Setup (D) can also be classified into two types according to the lens used. This experiment will compare the differences in structured illumination microscopy imaging between these two experimental setups.

The experimental methodology for this experiment is as follows. These three different setups were reconstructed through the three angles of the illumination pattern, which is

0, 60, 120 degree. The middle result has a higher frequency and the remaining two have similar frequencies. Since setup (A) and setup (D) use different numbers of lenses and setup (D) contains a mask, the loss of power in the optical path is different. Therefore setup(A) uses a laser with an intensity $-5dBm$ and setup(D) uses a laser with an intensity $0dBm$.

The plotting method used in this and subsequent experiments is to take the average value of the plot, which makes the curve smoother, avoids the interference of error points, and makes the characteristics more obvious. We need the contrast of the image, which can be done as follows. Average the intensity of pixel points in the image that are parallel to the target bright line, and then plot the intensity of each average value sequentially in order of perpendicularity to the bright line.

RESULT AND DISCUSSION

We measure the light intensity of $-5dBm$ using experimental setup A and the image recorded is shown in figure3.5.(b) and figure3.5.(c). Analyzing the horizontal line under the smallest figure to compare the contrast, we find that the structured illumination microscopy obtained by setup(A) has a small enhancement of the contrast: contrast ratio increased by 3% based on the maximum light intensity, which is shown in figure3.5. (h). Meanwhile, analyzing the image obtained by setup(D) with a small magnification scale of lens in the same way, we can also see that the structured light microscopy has little enhancement on the contrast of around 5% shown in figure3.5.(i). However, the image obtained from setup(D) with a large magnification ratio shows that the structured light microscope provides a large contrast enhancement around 31.5% shown in figure3.5.(j). Note that the different experimental setups are all imaging at the most precise level achievable for this setup. Depending on the group 1 element 2 or 3 that most clearly images the 1951 USAF resolution chart, this yields a camera resolution of $2.24lp/mm - 2.52lp/mm$, and the spatial frequency of the illumination is about $3.33lp/mm$.

The structural illumination achieved by direct modulation of the incident light is not well realized for structural illumination microscopy, which may be due to the lack of contrast in the illumination pattern and background noise. Secondly, structured illumination microscopy achieved by diffraction enables super-resolution imaging and solves the out-of-focus problem, which is shown in element 3 in figure3.5. (d). The large contrast enhancement obtained by setup(D) with a large magnification factor proves that super-resolution imaging is achieved. Meanwhile, comparing figure3.5(d) and 3.5(e), we can see that the out-of-focus problem of the horizontal line after the number 3 in figure3.5(d) is well improved in figure3.5(e).

3.3.2. EFFECT OF ILLUMINATION FREQUENCY AND ANALYSIS

This experiment compares the effect of different spatial frequencies of structured illumination patterns on structured illumination imaging.

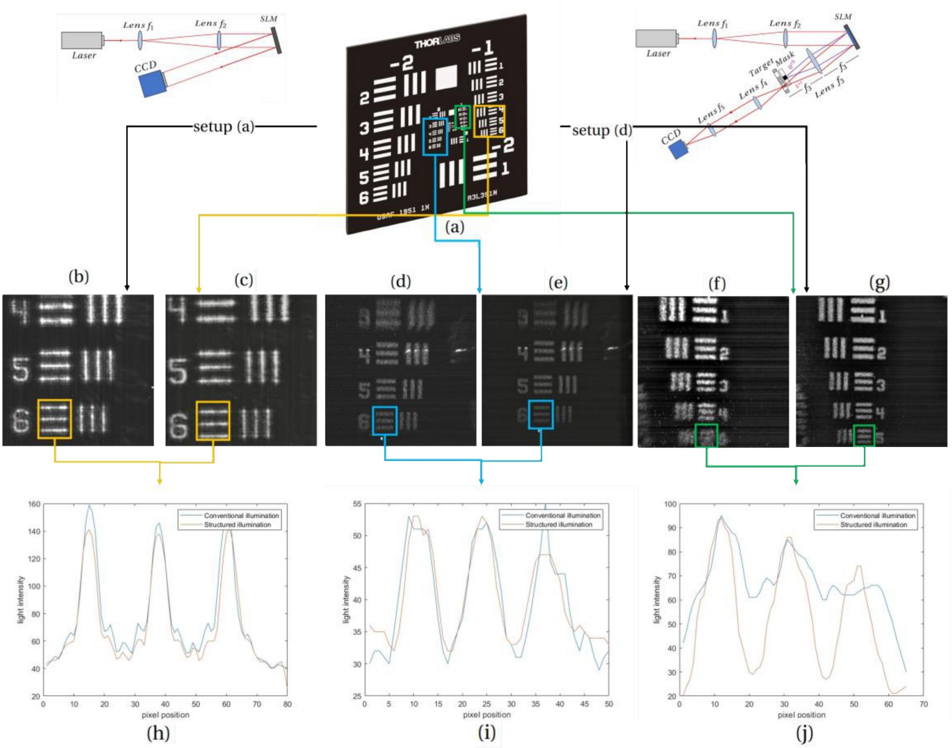

Figure 3.5: Effect of experimental setup. The position of the imaging target in the resolution target is shown in figure (A). The final SIM image of the experimental setup (A) is shown in figure (c), and the image of the system with wide field illumination is shown in figure (b). The final SIM image of the experimental setup (D) and a small focal length lens selected is shown in figure (e), and the image of the system with wide field illumination is shown in figure (d). The final SIM image of the experimental setup (D) and a large focal length lens is shown in figure (g), and the image of the system with wide field illumination is shown in figure (f). The contrast results of the imaging obtained by the three experimental setups with or without structured illumination are shown in (h), (i), and (j).

Theoretically, suppose the frequency of the structured illumination light is increased. In that case, the object imaged by the structured illumination light will have an increased offset in the frequency domain, which means that the camera can pick up more information. Thus the quality of the reconstructed image will be higher.

EXPERIMENTAL METHODS

The experimental method for this experiment is as follows. We used setup (D) with a laser of intensity 0 dBm. Moreover, we used the illumination pattern through three different rotation angles for SLM imaging in the experiment, and the angles were taken as 0, 60, and 120 degrees, respectively. The spatial frequency of the illumination pattern used in figure3.8(b) is $3.3lp/mm$. The spatial frequency of the illumination pattern used in figure3.8(c) is $2.2lp/mm$. The spatial frequency of the illumination pattern used in figure3.8(d) is $1.1lp/mm$.

The illumination pattern was obtained by presenting the diffraction pattern of figure3.7 on the SLM. Other illumination patterns were obtained by scaling and rotating figure3.7. figure3.6 shows the optical-transfer function (OTF) of setup(D). Since the camera is located in the Fourier plane, the OTF of the system can be obtained directly when the illumination pattern is not modulated in any way, and the resolution chart and mask are removed.

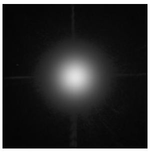

Figure 3.6: OTF of the system

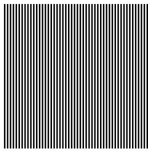

Figure 3.7: Original illumination pattern

RESULT AND DISCUSSION

In the figure3.8, we can see element 5 when the illumination spatial frequency is highest, while at the lowest, element 5 is quite blurred. Therefore, we find that the spatial frequency increase from $1lp/mm$ to $3.3lp/mm$, the high-frequency structured illumination improves the contrast about 35%, and improves the resolution of the image from $2.83lp/mm$ to $3.17lp/mm$.

In conclusion, we show that the higher the frequency of structural illumination, the higher contrast and resolution imaging is achieved.

3.3.3. EFFECT OF INPUT ANGLE AND ANALYSIS

In theory, if the image is reconstructed using three angles, then the superposition pattern

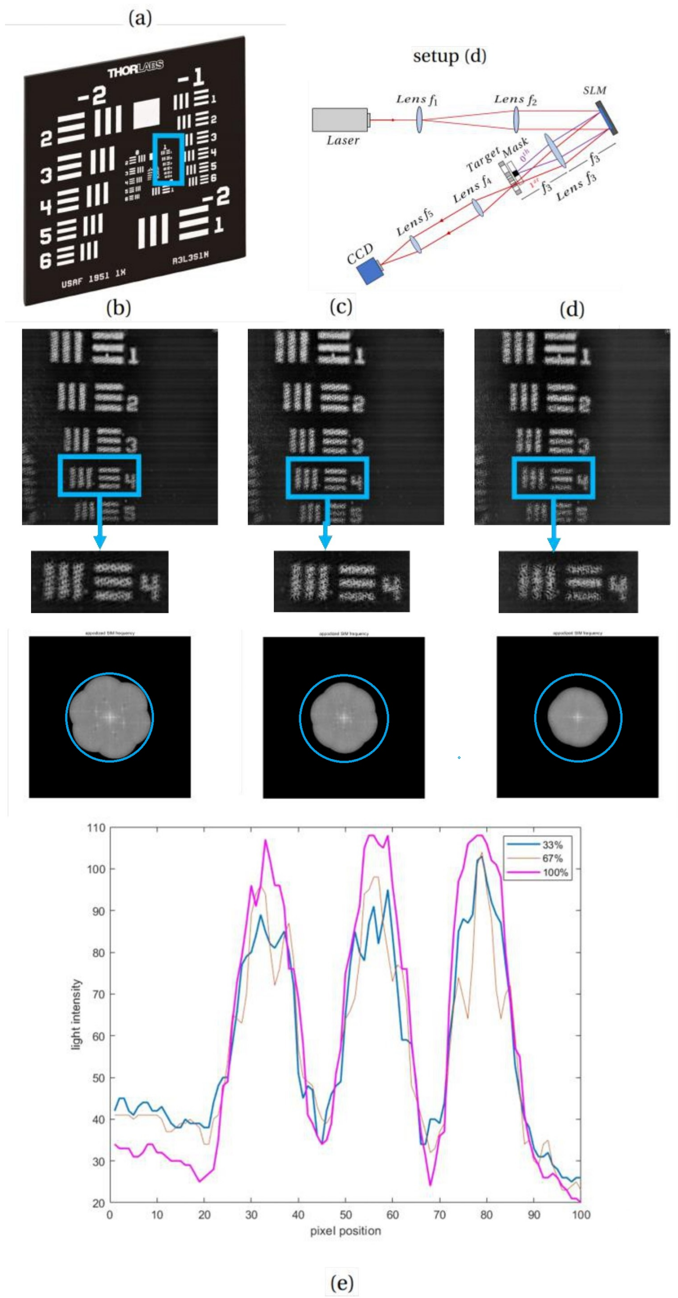

Figure 3.8: Effect of illumination frequency and analysis. The SIM image of the setup(D) and a large focal length lens at the same part of resolution target(a) is shown in figure(b)-(d). The spatial frequency of the structural illumination pattern used to image figure (b) is the highest. The frequency of the structured illumination pattern for imaging figure (c) is reduced by 17 percent compared to figure (b), and the frequency of the structured illumination pattern for imaging figure (d) is reduced by 33 percent compared to figure (c). The blue circles in the figure are circles of the same size and serve as a scale.

obtained in the frequency domain should be an overlap of six circles. Then if more angles are utilized to reconstruct the image, the coverage area of the superimposed figure in the frequency domain will become larger and gradually converge to a large circle, leading to a higher resolving power.

EXPERIMENTAL METHODS

The experimental method for this experiment is as follows. We used setup (D) with a laser of intensity $0dBm$. The spatial resolution of the illumination pattern is $3.3lp/mm$. The angles were taken as 0, 60, and 120 degrees in the experiments of SLM imaging by illuminating patterns with three different rotation angles. In the experiments of illumination patterns through six different rotation angles, the angles were taken as 0, 30, 60, 90, 120, and 150 degrees, respectively. In the experiments with illumination patterns through nine different rotation angles, the angles were taken as 0, 20,40, 60, 80, 100, 120, 140, 160degrees.

RESULT AND DISCUSSION

In figure3.9(e), we compared the contrast of the reconstructed super-resolution image obtained through 9 angles, as shown by the orange line, and the reconstructed super-resolution image obtained through 3 angles, as shown by the blue line. It is clear that more angular reconstruction results in images with higher contrast and higher clarity and image quality.

In conclusion, we showed that by reconstructing the image through more angles, we can get a structural illumination image with higher resolution.

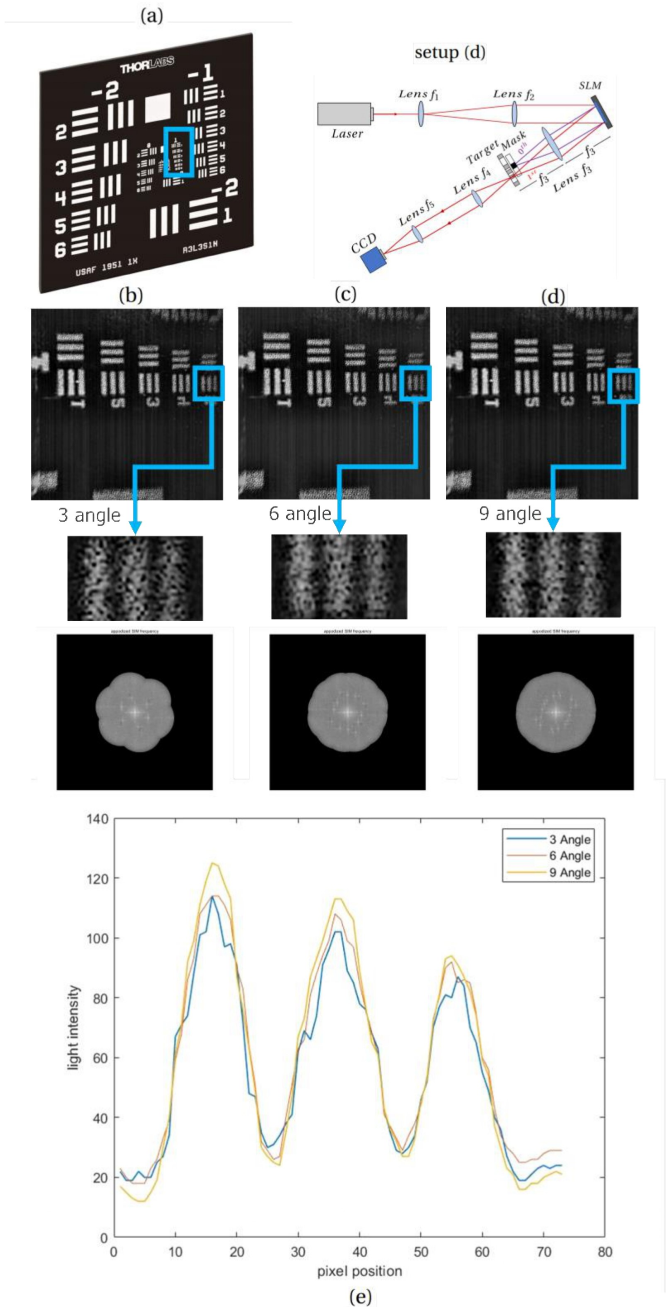

Figure 3.9: Effect of input angle and analysis. The SIM image of the setup(D) and a large focal length lens at the same part of resolution target(a) is shown in figure(b)-(d). Figure (b)-(d) shows the SIM imaging obtained by inputting three different angles of the structural illumination pattern. Figure (e) shows the comparison of the image contrast of the final reconstructed SIM image now with the horizontal line after the smallest digit for different reconstruction angles.

4
IMPROVEMENT OF STRUCTURED ILLUMINATION IN SCATTERING MEDIUM

This chapter starts with an introduction to algorithms for solving the scattering problem in the first and second sections and an algorithm is obtained that optimises the scattering problem. The results of the algorithm are presented and analysed in the third section.

4.1. POTENTIAL METHODS FOR IMPROVEMENT IN SCATTERING MEDIA

This section focuses on techniques potentially enhancing structured illumination in scattering media. According to literature research, the effects of scattering can be improved by machine learning or other techniques while increasing resolution. A discussion of these techniques is given.

4.1.1. MACHINE LEARNING METHODS

”Machine learning" refers to the process of applying predictive models to data or of finding informative clusters within data[37]. Machine learning has grown significantly over the past several years and has many applications. Machine learning is encouraged at both pre-clinical and clinical stages since in terms of medical imaging technologies, medical data processing, medical diagnosis, and other healthcare issues, it offers a lot of promise[38].

NEURAL NETWORK

Deep learning (DL), also known as data-driven artificial neural networks, has strengths in extracting intricate patterns from vast amounts of data to select the ideal solution in the parameter space[39]. Deep learning has an outstanding performance in the problem of image processing[38]. As a result, this is well suited to the analysis of complex situations where the scattering process is learned from before and after images of scattering.

A convolutional network, in its simplest form, is an input-to-output mapping that is capable of learning different mapping connections between inputs and outputs without the necessity for precise mathematical expressions between inputs and outputs. As long as a training set (known pictures or data) is used to train the convolutional network, it can map between input-output pairs. The mapping relationship between the image before and after scattering is constructed through the neural network so that when the image after scattering is obtained, the image before scattering can be obtained according to the mapping relationship, and in this way, the effect of scattering on photoacoustic imaging with the application of structured illumination can be reduced. Consequently, neural networks can directly address the issue of scattering and improve low-quality images. However, it cannot obtain a function for the scattering process.

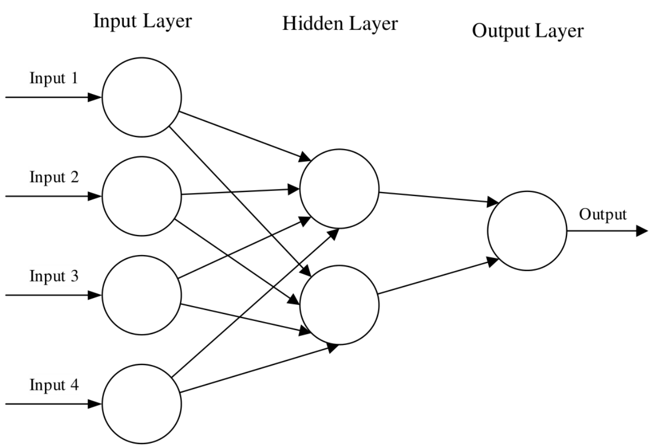

Figure 4.1: Simple structure of artificial neural network[40]

Figure4.1 shows the traditional artificial neural network (ANN). The input would be distributed to the hidden layers after being loaded into the input layer. The target affects the inputs and results. The input and output in this study are the image before scattering and the picture in the scattering medium, respectively. The hidden layers determine whether a stochastic change inside themselves negatively impacts or improves the output throughout the learning process by taking into account judgements from the previous layer.[40]. Deep learning is a term used to describe the stacking of many hidden layers.

Convolutional neural networks(CNN) are a target type of deep learning. CNNs differ from classical ANNs in that it has a more efficient way of connecting neurons. Therefore, CNN is no longer a one-to-one connection of all data information. Instead of receiving input from the whole preceding layer, the buried neurons in the following layer only get input from the corresponding part(input from the previous neuron)[41]. As a result, CNN works best with image-like data with some local structure, and when identifying such structure is a primary goal of the research[37]. Correspondingly, our research aims to optimize the imaging of structured illumination, and this is to optimize the local information of the image (the target to be imaged).

The composition of a CNN is as follows. The input to the CNN is available in three dimensions of length, width, and height, which can be the 2D pixels and colour depth of the input scattered image[41]. There are three different kinds of layers in CNNs, namely the convolutional, the pooling, and the fully connected layers.[41].

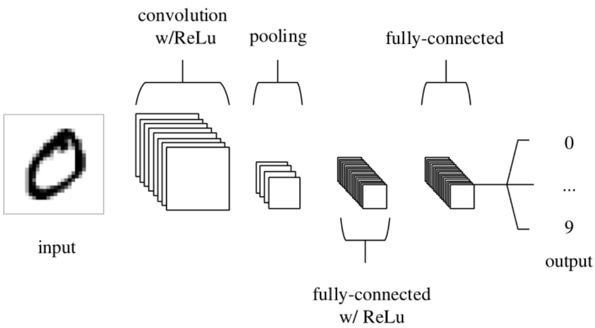

Figure 4.2: Simple structure of CNN[40]

The system is trained on a training dataset using this approach. The scattered image is input at the input port, and the CNN is used to obtain the mapping by a given size (the range of sizes of the convolution) and step size (the length of each convolution span). The network uses a loss function to determine the discrepancy between the output and the actual value, which is utilized to direct the model's training. In using CNNs to optimize scattered images, The training phase of the scattered before-and-after mapping model may require up to 1000 photos[42].

4.1.2. OTHER METHODS

In addition to machine learning, many other methods can be used to ameliorate the effects of scattering.

One option is electronic confocal slit detection (CSD). When imaging scattering samples with SI, the image signal-to-noise ratio (SNR) dropped at high pattern frequencies. The higher optical sectioning performance of SI could be accomplished while still preserving high picture SNR by combining eCSD with SI to lower background signal and noise[43].

Imaging in highly scattering solutions can also be enhanced by combining SI with a spatial Fourier filter. When combined, spatial Fourier filtering and structured illumination provide an significantly image contrast[44]. However, this picture enhancement comes at the expense of some high spatial frequencies being lost and light intensity being decreased[44].

At the same time, the issue can be resolved using only physical means. Longer wavelength structural illumination is substantially less prone to scattering. Adding Optical clearing-aided is also another way to achieve this. Glycerol is suggested to be used as an optical clearing agent to lessen tissue scattering, and both in vitro and in vivo imaging performance of imaging can be significantly improved by optical clearing[45].

Compared to other machine learning methods, neural networks are more suitable for learning large-scale data, and convolutional neural networks have strong performance in processing images because the convolution operation reduces the computation. Moreover, the combination of CNN can avoid sample contamination and significantly improve the scattering effect through operable methods. Thus, this section will explore CNN to improve structural illumination in scattering medium.

However, for neural networks to learn, they also need more data. In the neural network technique, the rate at which the experimental apparatus generates data becomes crucial.

4.2. CNN ALGORITHMIC PRINCIPLE

This section first introduces the super-resolution CNN algorithm on which this study is based and presents the main reference algorithmic framework: single-image super-resolution (SISR). Furthermore, the mathematical principles underlying the algorithm used in this study are presented. Lastly, the principle of the USRNet algorithm in this study is presented.

4.2.1. SISR

The process of converting low-resolution observations of the same scene into high-resolution photographs is known as super-resolution (SR)[46].Super-resolution based on deep convolutional networks is a rapidly expanding field with many useful applications.[47]. The super-resolution Convolutional Neural Networks could be divided into single-image super-resolution (SISR) and multi-image super-resolution (MISR) depending on the quantity of input low-resolution pictures[48].SISR is more popular than MISR due to its great effectiveness. High perceptual quality HR images are used widely in a variety of fields, including security imaging, satellite imaging, and medical imaging, because they include more useful details[48].

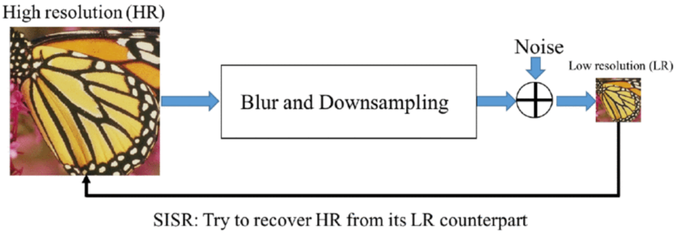

Figure 4.3: Sketch of the framework of SISR[48]

In the typical SISR framework for a scale factor of s, as depicted in figure4.3, the low-resolution (LR) image is a blurred, decimated, and noisy version of a high-resolution (HR) image. The method of SISR used in the study of this paper assumes that the blurred image y (in this study the image after scattering) is a complex degradation of the original real image x. Mathematically it can be expressed as[48]:

$$y = (x \otimes k)\downarrow_s + n, \tag{4.1}$$

where $\otimes$ is the convolution between the blurry kernel k and the unknown HR image x. The blurry kernel represents how blurred image is blurred, which is the scattering equation in this study. $\downarrow_s$ denotes s-fold downsampling, that means retaining the upper-left element of each distinct $s \times s$ and discarding the others, which is a kind of reduced sampling operator. n is usually the standard deviation (or noise level). The goal of SISR in this study is to be able to obtain original real image (before scattering image) from blurred image (after scattering image) by training the dataset with an unknown fuzzy kernel as input.

4.2.2. ALGORITHMIC FOUNDATION

HALF QUADRATIC SPLITTING(HQS)

Using HQS can insert the CNN denoiser trained by discriminative learning method as a module into the model-based optimization method to solve the fuzzy problem. Moreover, HQS has the property of being able to converge faster, making network learning easier[49].

General form of the image recovery objective function[50]:

$$\hat{x} = \arg\min_x \frac{1}{2} \parallel y - (x \otimes k) \downarrow_s \parallel^2 + \lambda \Phi(x), \quad x, y \in \mathbb{R}^{N \times M}. \tag{4.2}$$

$\hat{x}$ is the objective function that needs to be minimized. y is the fuzzy picture and x is the clear picture. This is also equivalent:

$$\hat{x} = \arg\min_x \frac{1}{2} \parallel y - (z \otimes k) \downarrow_s \parallel^2 + \lambda\Phi(x) \quad \text{s.t.} \quad z = x, \qquad z, x \in \mathbb{R}^{N\times M}. \tag{4.3}$$

HQS minimizes the above equation by solving the following cost function. This is obtained by augmenting the Lagrangian method. The augmented Lagrange multiplier method solves the problem of finding the minimum by finding x_{k+1} and z_{k+1} one at a time and then updating the parameter μ, gradually increasing μ with each iteration[51].

$$L_\mu(x,z) = \frac{1}{2} \parallel y - (z \otimes k) \downarrow_s \parallel^2 + \lambda\Phi(x) + \frac{\mu}{2} \parallel z - x \parallel^2, \qquad z, x \in \mathbb{R}^{N\times M}, \mu \in \mathbb{R}^+. \tag{4.4}$$

Which:

$$\begin{cases} z_{k+1} = \arg\min_z \frac{1}{2} \parallel y-(z \otimes k) \downarrow_s \parallel^2 + \mu \parallel z - x_k \parallel^2, \\ x_{k+1} = \arg\min_x \frac{\mu}{2} \parallel x - z_{k+1} \parallel^2 + \lambda\Phi(x). \end{cases} \tag{4.5}$$

U-NET AND RESIDUAL NETWORK(RESNET)

U-net is a neural network architecture. Its use in medical imaging is exploding[52]. The U-net network is composed of two different parts, the first of which is a contraction path built using a standard CNN design. Each block in the contraction path is made up of two $3x3$ convolutions that follow one another. This arrangement is repeated several times. the novelty of the U-net appears in the second part, called the expansion path, where each stage uses 2×2 upper convolutions. The feature maps of the corresponding layers in the contraction path are then cropped and connected to the upsampled feature maps. This is followed by two consecutive 3×3 convolutions and ReLU activation. Another $1 - times - 1$ convolution is used in the last step to divide the image and decrease the feature map to the required number of channels. This results in a network that resembles a U-shape, and this also propagates contextual information along the portions of the network that overlap.. Figure 4.4 illustrates the entire U-net architecture.In figure4.4, the arrows indicate the different operations, the blue boxes indicate the feature maps for each layer, and the gray boxes indicate the feature maps cropped in the contraction paths.

ResNet is a neural network based on the traditional neural network, instead of letting the "layer" output the final result, let the "layer" output the difference between the final result and the input features. The difference is added to the input features at the element level to get the final result.As shown in the figure4.5. There is better performance in very deep convolutional networks compared to traditional CNNs.

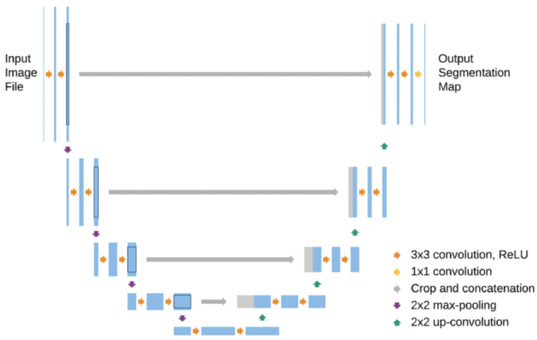

Figure 4.4: U-net framework

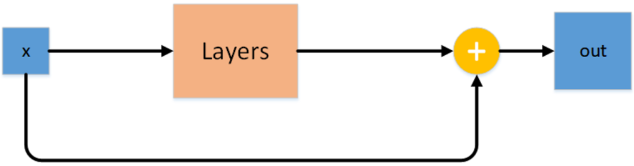

Figure 4.5: ResNet framework

4.2.3. USRNET

According to equation4.1, we can get that if we want to optimize the blurred image, then our goal is to minimize the following equation.

$$\arg\min(x \otimes k)\downarrow_s - y \tag{4.6}$$

This can be equated to minimizing the following function:

$$F(x) = \arg\min_x \frac{1}{2\sigma^2} \parallel y - (x \otimes k)\downarrow_s \parallel^2 + \lambda\Phi(x) \tag{4.7}$$

According to the HQS algorithm, we can iteratively solve the following equation4.8 to obtain the minimum value of the above equation4.7.

$$L(x,z) = \frac{1}{2\sigma^2} \parallel y - (z \otimes k)\downarrow_s \parallel^2 + \lambda\Phi(z) + \frac{\mu}{2} \parallel z - x \parallel^2 \tag{4.8}$$

Which:

$$\begin{cases} z_{k+1} = \arg\min_z \frac{1}{2} \parallel y-(z\otimes k)\downarrow_s \parallel^2 + \mu\sigma^2 \parallel z - x_k \parallel^2, \\ x_{k+1} = \arg\min_x \frac{\mu}{2} \parallel x - z_{k+1} \parallel^2 + \lambda\Phi(x). \end{cases} \tag{4.9}$$

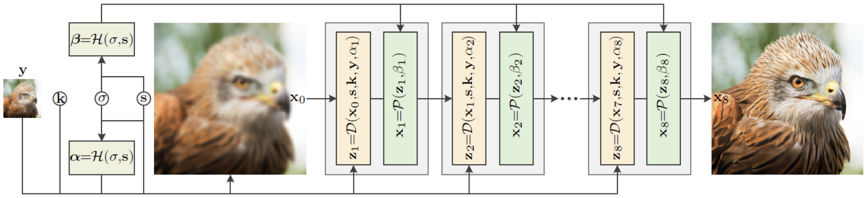

Figure 4.6: USRNet framework[50]

Figure4.6 shows the network framework and we give an example of 8 iterations. We define for k^{th} iteration, denoted by the footnote $_k$, $\alpha_k = \mu_k\sigma^2$ and $\beta_k = \sqrt{\lambda/\mu_k}$. Starting from the obtained fuzzy picture y. The first iteration is x_1 and z_1. The function D means that z_1 passes through a weighted combination of the minimization data term $\parallel y-(z\otimes k)\downarrow_s \parallel^2$ and $\parallel z - x_k \parallel^2$, which is also known as the minimization of equation4.9. The result is to find a sharper image.The hyperparameter module H acts as a slider to control the outputs of the data module and the previous module.For instance, as α_k increases, the solution z_k will be progressively closer to x_{k-1}. The function P indicates that z_k is passed through a noise reducer with a noise level β_k to obtain a sharper image x_{k-1}, which is the solution to Equation4.9. In addition, it contains a deep CNN noise reducer with noise level as input. This noise reducer is realized by ResUNet, integrating the residual block into U-Net. ResUNet takes z_k as inputs and outputs the denoised image x_{k-1}.

4.3. EXPERIMENT AND RESULTS

4.3.1. EXPERIMENTAL SETUP AND SOFTWARE SETTINGS

The experimental setup used in this experiment is a modification of setup (D). It remove the resolution target and add a scattering medium after the lens,which shown in figure4.7.

In this experiment, a plastic sheet is used as the scattering medium, and the surface of the folded plastic sheet consists of a huge number of tiny planes with different tilt angles, and the plastic sheet itself can scattering.

The programming language used for this experiment is Python. Python, a widely adopted programming language, plays a pivotal role in academia due to its user-friendly syntax and rich libraries. PyTorch is an open-source machine-learning framework with an

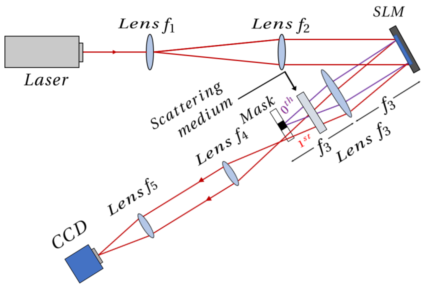

Figure 4.7: Experimental setup

adaptable and intuitive design.PyTorch belongs to an integrated feature of Python and follows the grammar of Python. It is well suited for complex neural network training, which is needed for this study because of the large amount of data for image as data training.

The version of Python for this experiment is 3.7.16, and the version of Pytorch is 1.7.0. Note that the code used in this experiment does not apply to Pytorch after 1.7.0. This experiment was trained by images of sinusoidal patterns with different angles and all spatial frequencies of $3.3lp/mm$. The training dataset includes 200 pairs of before and after scattering images. The testing data is $3lp/mm$ images, whose frequency is lower than the training set.

4.3.2. EXPERIMENTAL RESULTS AND DISCUSSION

The spatial resolution of the testing data is $3lp/mm$ images. The experiments test the improved capabilities of USRNet while also comparing the differences between USRNet and ESRGAN, a now popular super-resolution imaging method.

ESRGAN(Enhanced Super-Resolution Generative Adversarial Network) employs advanced neural networks, specifically Generative Adversarial Networks (GANs), to significantly improve image resolution and quality. The ESRGAN applied in this experiment directly utilises the already trained super-resolution model, which is based on the principle of transforming low-resolution images into high-resolution images. This process does not involve the learning of scattering processes.

The images of the experimental results are shown in the figure4.8. The results are evaluated by calculating the peak signal-to-noise ratio (PSNR), signal-to-noise ratio (SNR) and structural similarity index measure (SSIM) of the images. The reference object for calculating PSNR, SNR and SSIM is the original image.

From the results in table4.1, we can see that for the original image, PSNR and SNR are infinite (Inf), while SSIM is 1. The original graph is a reference for calculating PSNR, SNR

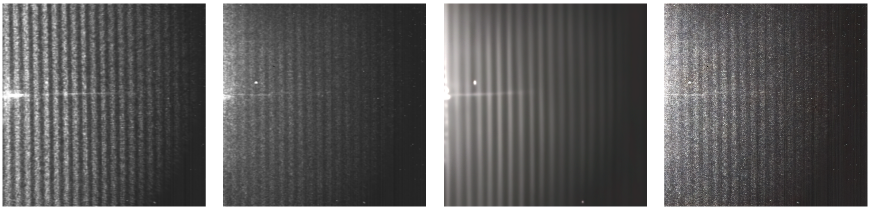

(a) (b) (c) (d)

Figure 4.8: USRnet and ESRGAN improvements for scattering imaging. Figure(a) is original image, and (b) is Scattering image. Figure(c) is the result after improvement through USRNet, and (d) is the result after improvement through ESRGAN.

Table 4.1: The results of PSNR (dB), SNR (dB) and SSIM

	Original image	**Scattering image**	**USRNet**	**ESRGAN**
PSNR	Inf	17.0141	19.1482	17.8651
SNR	Inf	8.4808	10.6149	9.3317
SSIM	1	0.1901	0.3467	0.2045

and SSIM. By comparing the analysis results of the scattered images with the optimised images of USRNet and ESRGAN, we can find that the value of USRNet is the highest of the three, which means that USRNet has a clearer image and a structure more similar to the original image. Comparing ESRGAN and the scattered image, we can find that although ESRGAN improves the quality of the image, it is less significant than USRNet.

5

Discussion and recommendations

This chapter reviews the previous experimental methods and results and suggests future improvements. Furthermore, this chapter also writes about the future outlook, with feasible future directions.

Conclusion

Overall we found that the setup had an influence. the experimental setup of SLM by diffraction imaging can achieve better structural illumination imaging due to its ability to realize structural illumination patterns better. Moreover, the addition of angles in imaging improved the image contart by obtaining more information in the frequency domain. Furthermore, increasing the frequency in imaging also improves the contrast of the image due to the ability to obtain a wider range of frequency domain information.

Methodological improvement

The experimental methodology of this experiment leaves much to be desired. We can find that there is still residual zero-order diffraction in the experimental image. Moreover, in terms of optimising the illumination pattern after scattering, the outlines of the optimised pictures still need to be enhanced.

Zero-order diffraction In this experiment, because the mask size is fixed, there is no way to mask all the zero-order diffraction when the light intensity or experimental setup changes. In contrast, projecting another correction beam to cancel with the zero-order diffraction is more flexible and can be modulated at any time according to different zero-order diffraction. This method has also been validated, and the correction beam can be derived algorithmically when the intensity and phase in the Fourier plane are known[28]. We know that the zero-order diffraction is due to dead zones on the SLM, and the corrected light speed produces an equal amount of light from the phase-modulated region of the SLM to cancel out the zero-order beam caused by the SLM dead zones[28].

CNN In the results of this experiment, we can find that USRNet has more coherent stripe shapes but with fuzzy outlines, whereas the results obtained by ESRGAN still resemble discrete points scattered but with clearer outlines.

Due to the time limitations of the study, we did not train ESRGAN. Future research could train models for the inverse scattering problem by studying the principles of ESRGAN on it. Exploring the inverse scattering model that combines SRGAN with USRNet is a worthy direction for future research.

RESULTS IMPROVEMENT

In the section on the Effect of input angle and analysis, we can find that in figure3.9(e), although we can see the increase in contrast due to the increase in angle, the magnitude of the increase is insignificant. Future experiments could study the increase in angle with smaller objects or lower spatial frequency illumination patterns.

FUTURE OUTLOOK

photoacoustic microscopy (PAM) has various applications in clinical research and basic biology for studying diseases. Deep imaging depth is an excellent advantage of PAM over conventional microscopy, but it have the out-of-focus problem. In the scattering medium, optical scattering[53] and ultrasonic scattering[54][55] can have an effect on imaging[56]. SIM technologies can be applied in PAM. it can be applied to improve the out-of-focus area of the PAM[12]. However, the combined SIM and PAM technique is more easily affected by scattering.

The present study aimed to build an experimental setup for structural illumination imaging and to solve the problem of structural illumination patterns in scattering media. Future research can be based on this study to achieve clear imaging in scattering medium. In addition, solving the scattering problem in the combination of PAM and structured illumination is also a worthy research direction in the future.

Bibliography

[1] Manish Saxena, Gangadhar Eluru, and Sai Siva Gorthi. “Structured illumination microscopy”. In: *Advances in Optics and Photonics* 7.2 (2015), pp. 241–275.

[2] Rainer Heintzmann and Thomas Huser. “Super-resolution structured illumination microscopy”. In: *Chemical reviews* 117.23 (2017), pp. 13890–13908.

[3] Mats GL Gustafsson. “Surpassing the lateral resolution limit by a factor of two using structured illumination microscopy”. In: *Journal of microscopy* 198.2 (2000), pp. 82–87.

[4] Florian Ströhl and Clemens F Kaminski. “Frontiers in structured illumination microscopy”. In: *Optica* 3.6 (2016), pp. 667–677.

[5] Alice Sandmeyer et al. “DMD-based super-resolution structured illumination microscopy visualizes live cell dynamics at high speed and low cost”. In: *BioRxiv* (2019), p. 797670.

[6] Yanquan Mo et al. “Structured illumination microscopy artefacts caused by illumination scattering”. In: *Philosophical Transactions of the Royal Society A* 379.2199 (2021), p. 20200153.

[7] Maria Ingaramo et al. “Two-photon excitation improves multifocal structured illumination microscopy in thick scattering tissue”. In: *Proceedings of the National Academy of Sciences* 111.14 (2014), pp. 5254–5259.

[8] Peter W Winter et al. “Two-photon instant structured illumination microscopy improves the depth penetration of super-resolution imaging in thick scattering samples”. In: *Optica* 1.3 (2014), pp. 181–191.

[9] Elias Kristensson, Edouard Berrocal, and Marcus Aldén. “Quantitative 3D imaging of scattering media using structured illumination and computed tomography”. In: *Optics Express* 20.13 (2012), pp. 14437–14450.

[10] Yicong Wu and Hari Shroff. “Faster, sharper, and deeper: structured illumination microscopy for biological imaging”. In: *Nature methods* 15.12 (2018), pp. 1011–1019.

[11] Ying Ma et al. “Recent advances in structured illumination microscopy”. In: *Journal of Physics: Photonics* 3.2 (2021), p. 024009.

[12] Jiamiao Yang et al. “Motionless volumetric photoacoustic microscopy with spatially invariant resolution”. In: *Nature communications* 8.1 (2017), pp. 1–7.

[13] P Burgholzer et al. “Photoacoustic super-resolution microscopy using blind structured speckle illumination”. In: *Photons Plus Ultrasound: Imaging and Sensing 2017*. Vol. 10064. SPIE. 2017, pp. 337–341.

[14] Mohammadreza Amjadian et al. “Super-resolution photoacoustic microscopy using structured-illumination”. In: *IEEE Transactions on Medical Imaging* 40.9 (2021), pp. 2197–2207.

[15] Mohammadreza Amjadian et al. “Super-resolution photoacoustic microscopy via modified phase compounding”. In: *IEEE Transactions on Medical Imaging* 41.11 (2022), pp. 3411–3420.

[16] Neil Savage. *Digital spatial light modulators*. 2009.

[17] John A Neff, Ravinda A Athale, and Sing H Lee. “Two-dimensional spatial light modulators: a tutorial”. In: *Proceedings of the IEEE* 78.5 (1990), pp. 826–855.

[18] Uzi Efron. *Spatial light modulator technology: materials, devices, and applications*. Vol. 47. CRC press, 1994.

[19] Kristina M Johnson, Douglas J McKnight, and Ian Underwood. “Smart spatial light modulators using liquid crystals on silicon”. In: *IEEE Journal of Quantum Electronics* 29.2 (1993), pp. 699–714.

[20] Stirling Scholes et al. “Structured light with digital micromirror devices: a guide to best practice”. In: *Optical Engineering* 59.4 (2020), pp. 041202–041202.

[21] Sergey Turtaev et al. “Comparison of nematic liquid-crystal and DMD based spatial light modulation in complex photonics”. In: *Optics express* 25.24 (2017), pp. 29874–29884.

[22] Tao Xian and Xianyu Su. “Area modulation grating for sinusoidal structure illumination on phase-measuring profilometry”. In: *Applied Optics* 40.8 (2001), pp. 1201–1206.

[23] Philipp J Keller et al. “Fast, high-contrast imaging of animal development with scanned light sheet–based structured-illumination microscopy”. In: *Nature methods* 7.8 (2010), pp. 637–642.

[24] Joseph W Goodman. *Introduction to Fourier optics*. Roberts and Company publishers, 2005.

[25] Prof. George Barbastathis. *Optics*. Available at `https://ocw.mit.edu/courses/2-71-optics-spring-2009/` (2019/03/01).

[26] Emiliano Ronzitti et al. “LCoS nematic SLM characterization and modeling for diffraction efficiency optimization, zero and ghost orders suppression”. In: *Optics express* 20.16 (2012), pp. 17843–17855.

[27] V Arrizon, E Carreon, and M Testorf. “Implementation of Fourier array illuminators using pixelated SLM: efficiency limitations”. In: *Optics communications* 160.4-6 (1999), pp. 207–213.

[28] Darwin Palima and Vincent Ricardo Daria. “Holographic projection of arbitrary light patterns with a suppressed zero-order beam”. In: *Applied optics* 46.20 (2007), pp. 4197–4201.

[29] EZ Zhang et al. “In vivo high-resolution 3D photoacoustic imaging of superficial vascular anatomy”. In: *Physics in Medicine & Biology* 54.4 (2009), p. 1035.

[30] Minchol Lee, Donghoon Koo, and Jeongmin Kim. “Simple and fast calibration method for phase-only spatial light modulators”. In: *Optics Letters* 48.1 (2023), pp. 5–8.

[31] Amar Deo Chandra and Ayan Banerjee. “Rapid phase calibration of a spatial light modulator using novel phase masks and optimization of its efficiency using an iterative algorithm”. In: *Journal of Modern Optics* 67.7 (2020), pp. 628–637.

[32] Jianpei Xia et al. “Pixel-addressable phase calibration of spatial light modulators: a common-path phase-shifting interferometric microscopy approach”. In: *Journal of Optics* 19.12 (2017), p. 125701.

[33] Rujia Li, Yunhui Gao, and Liangcai Cao. “In situ calibration for a phase-only spatial light modulator based on digital holography”. In: *Optical Engineering* 59.5 (2020), pp. 053101–053101.

[34] GJ Dijk. “Intensity Patterns Generated with a Spatial Light Modulator”. PhD thesis. Master’s thesis, Eindhoven University of Technology, 2012.

[35] Nadya Chakrova. “Versatile Structured Illumination Microscopy”. In: (2017).

[36] Amit Lal, Chunyan Shan, and Peng Xi. “Structured illumination microscopy image reconstruction algorithm”. In: *IEEE Journal of Selected Topics in Quantum Electronics* 22.4 (2016), pp. 50–63.

[37] Joe G Greener et al. “A guide to machine learning for biologists”. In: *Nature Reviews Molecular Cell Biology* 23.1 (2022), pp. 40–55.

[38] Changchun Yang et al. “Review of deep learning for photoacoustic imaging”. In: *Photoacoustics* 21 (2021), p. 100215.

[39] Ian Goodfellow, Yoshua Bengio, and Aaron Courville. *Deep learning*. MIT press, 2016.

[40] Keiron O’Shea and Ryan Nash. “An introduction to convolutional neural networks”. In: *arXiv preprint arXiv:1511.08458* (2015).

[41] Saad Albawi, Tareq Abed Mohammed, and Saad Al-Zawi. “Understanding of a convolutional neural network”. In: *2017 international conference on engineering and technology (ICET)*. Ieee. 2017, pp. 1–6.

[42] Ya Gao et al. “Deep learning-based photoacoustic imaging of vascular network through thick porous media”. In: *IEEE Transactions on Medical Imaging* 41.8 (2022), pp. 2191–2204.

[43] Bihe Hu, Daniel Bolus, and J Quincy Brown. “Improved contrast in inverted selective plane illumination microscopy of thick tissues using confocal detection and structured illumination”. In: *Biomedical Optics Express* 8.12 (2017), pp. 5546–5559.

[44] Edouard Berrocal, Sven-Göran Pettersson, and Elias Kristensson. “High-contrast imaging through scattering media using structured illumination and Fourier filtering”. In: *Optics letters* 41.23 (2016), pp. 5612–5615.

[45] Yong Zhou, Junjie Yao, and Lihong V Wang. “Optical clearing-aided photoacoustic microscopy with enhanced resolution and imaging depth”. In: *Optics letters* 38.14 (2013), pp. 2592–2595.

[46] Sung Cheol Park, Min Kyu Park, and Moon Gi Kang. “Super-resolution image reconstruction: a technical overview”. In: *IEEE signal processing magazine* 20.3 (2003), pp. 21–36.

[47] Saeed Anwar, Salman Khan, and Nick Barnes. “A deep journey into super-resolution: A survey”. In: *ACM Computing Surveys (CSUR)* 53.3 (2020), pp. 1–34.

[48] Wenming Yang et al. “Deep learning for single image super-resolution: A brief review”. In: *IEEE Transactions on Multimedia* 21.12 (2019), pp. 3106–3121.

[49] Yubao Sun et al. “Learning non-locally regularized compressed sensing network with half-quadratic splitting”. In: *IEEE Transactions on Multimedia* 22.12 (2020), pp. 3236–3248.

[50] Kai Zhang, Luc Van Gool, and Radu Timofte. “Deep unfolding network for image super-resolution”. In: *Proceedings of the IEEE/CVF conference on computer vision and pattern recognition*. 2020, pp. 3217–3226.

[51] Kuanhong Cheng et al. “Image super-resolution based on half quadratic splitting”. In: *Infrared Physics & Technology* 105 (2020), p. 103193.

[52] Nahian Siddique et al. “U-net and its variants for medical image segmentation: A review of theory and applications”. In: *Ieee Access* 9 (2021), pp. 82031–82057.

[53] Steven L Jacques. “Optical properties of biological tissues: a review”. In: *Physics in Medicine & Biology* 58.11 (2013), R37.

[54] Keith A Wear. “Ultrasonic scattering from cancellous bone: A review”. In: *IEEE transactions on ultrasonics, ferroelectrics, and frequency control* 55.7 (2008), pp. 1432–1441.

[55] SØ Aks and DJ Vezzetti. “Ultrasonic scattering theory. I: Scattering by single objects”. In: *Ultrasonic Imaging* 2.2 (1980), pp. 85–101.

[56] Yan Liu, Chi Zhang, and Lihong V Wang. “Effects of light scattering on optical-resolution photoacoustic microscopy”. In: *Journal of Biomedical Optics* 17.12 (2012), p. 126014.